Computational Modelling of the Phosphorylation Mechanism between ATP and Glucose

By © Andrew Walsh

A Thesis submitted

to the School of Graduate Studies in partial fulfillment of the

requirements for the degree of

Master of Science

Department of Chemistry

Memorial University of Newfoundland

August 2018

St. John's Newfoundland and Labrador

Abstract

Microbes have found ways to render certain drugs ineffective and hence are no longer susceptible to them. Continued misuse of a wide variety of drugs has given rise to organisms being able to resist them, which has led to multidrug resistance. One way to solve the issue of multidrug resistance is by looking at the mechanism of phosphorylation using adenosine triphosphate (ATP) the phosphate donor. If the phosphorylation of antibiotics can be prevented from occurring, then they would retain their antibacterial activity and thus help solve the issue of drug modification by bacteria.

The two-step mechanism for the phosphorylation of glucose using ATP, in which ATP is dephosphorylated in the first step and glucose is phosphorylated in the second step, is investigated using Hartree-Fock (HF) and B3LYP calculations with the 6-31G(d) and 6-31+G(d) basis sets. Glucose is chosen for study since it is a simple model for kanamycin. The ability of each conformer of ATP to donate a phosphate group is also discussed. The phosphorylation of both the alpha and beta anomers of glucose as well as the D and L enantiomers of glucose is also discussed.

It was determined that, while the chairPT isomer of ATP^{4-} is lower in energy than the chair isomer of ATP^{4-}, the ΔU_{rxn}, ΔH_{rxn} and ΔG_{rxn} values are less negative for the phosphorylation of the chair isomer of ATP^{4-}. The ΔU_{rxn}, ΔH_{rxn} and ΔG_{rxn} values are least positive for the phosphorylation of deprotonated β-L-glucose without water while they are least positive for the phosphorylation of deprotonated α-L-glucose upon inclusion of water molecules.

Keywords: phosphorylation, ATP, glucose

Acknowledgements

I would like to thank my supervisor, Dr. Ray Poirier, for all his guidance, knowledge and assistance with this project. I would also like to thank all the members of the Poirier research group for their help and support during this project.

I would also like to thank my supervisory committee members, Dr. Peter Warburton and Dr. Yuming Zhao for their contributions towards the completion of this project.

I would also like to thank Dr. Arpita Yadav and the members of her research group in the Department of Chemistry, University Institute of Engineering and Technology ChhatrapatiShahu Ji Maharaj University, Kanpur 208024 India for their collaboration and insight with this project and for sharing some of their data to use in Section 1.4 of this thesis as their work serves as the foundation of which this project is based upon.

I would like to acknowledge the Department of Chemistry, the School of Graduate Studies, Memorial University of Newfoundland and NSERC for funding towards this project.

I would also like to acknowledge Compute Canada, ACENET and WestGrid for the permission to use their computational resources for this project.

Table of Contents

Abstract ii

Acknowledgements iii

List of Tables vi

List of Figures viii

List of Schemes xi

List of Abbreviations and Symbols xii

List of Appendices xiii

Chapter 1 Introduction

1.1 Drug-resistant Compounds 1

1.2 ATP Phosphorylation 7

1.3 Conformers of ATP 13

1.4 Kanamycin Studies 15

1.4.1 Glucose, Neutral Kanamycin and a Simplified Model of Kanamycin 15

1.4.2 Variations of Neutral Kanamycin 18

1.5 Conformations of Glucose 22

Chapter 2 Methods

2.1 ATP and Glucose Conformers 26

2.2 Phosphorylation Reaction Products 28

2.3 Transition States 33

Chapter 3 Conformational Analysis and Dephosphorylation Mechanism of ATP^{4-}

3.1 Chair vs. Linear 35

3.2 A New Isomer of ATP^{4-} 37

3.3 Dephosphorylation of ATP^{4-} 39

3.3.1 Activation Energies 39

3.3.2 Energy Changes 45

3.3.3 Changes in Enthalpy, Entropy and Gibbs Energy 50

3.4 Feasibility of the ChairPT Isomer of ATP^{4-} 54

Chapter 4 Conformational, Anomeric and Isomeric Analysis and Phosphorylation Mechanism of the Glucose Anion

4.1 Conformational Analysis of the Glucose Anion 56

4.2 Anomeric and Isomeric Analysis of the Glucose Anion 58

4.3 A Different Isomer of the Glucose Anion 60

4.4 Phosphorylation of the Glucose Anion 61

4.4.1 Energy Changes 61

4.4.2 Changes in Enthalpy, Entropy and Gibbs Energy 63

4.5 Feasibility of Anomer and Isomer Conversions 68

4.5.1 Feasibility of the α-L-glucose Anion in the Phosphorylation Mechanism 68

4.5.2 Feasibility of the Proton Transfer Isomer of the Glucose Anion 72

Chapter 5 Conclusions 74

Bibliography and References 77

Appendices 83

List of Tables

Table 1.1 Docking Scores and Binding Energies for the Reactions of Kanamycin Derivatives with a) APH, ADP, Mg^{2+} and water and b) bacterial rRNA 20

Table 1.2 Docking Scores and Binding Energies for the Best Three Docking Poses of Kanamycin and Conjugate 3b with a) APH, ADP, Mg^{2+} and water and b) bacterial rRNA 21

Table 1.3 Zone of Inhibition of Kanamycin and Conjugate 3b Against Various Pathogenic Bacteria 21

Table 3.1 Relative Energies (in kJ mol^{-1}) of the Linear Conformer of ATP^{4-} with Respect to the Chair Conformer of ATP^{4-} 36

Table 3.2 Relative Energies (in kJ mol^{-1}) of the Proton Transfer Isomer of ATP^{4-} with Respect to the Chair Conformer of ATP^{4-} 38

Table 3.3 ATP^{4-} Dephosphorylation Activation Energies (in kJ mol^{-1}) 40

Table 3.4 ATP^{4-} Dephosphorylation Gibbs Energies of Activation (in kJ mol^{-1}) 43

Table 3.5 ATP^{4-} Dephosphorylation Energy Changes (in kJ mol^{-1}) 45

Table 3.6 Changes in Enthalpy for the Dephosphorylation of ATP^{4-} (in kJ mol^{-1}) 51

Table 3.7 Entropy Changes for the Dephosphorylation of ATP^{4-} (in J mol^{-1} K^{-1}) 51

Table 3.8 ATP^{4-} Dephosphorylation Gibbs Energy Changes (in kJ mol^{-1}) 52

Table 3.9 Enthalpy, Entropy and Gibbs Energy Changes for the Dephosphorylation of Chair ATP^{4-} With Water Included Using the HF/6-31G(d) level of theory. 53

Table 4.1 Energies of the Different Anomers of the Glucose Anion Relative to the β-D-glucose Anion (in kJ mol^{-1}) 59

Table 4.2 Changes in Energy for the Phosphorylation Mechanism of the Various Forms of the Deprotonated Glucose Anion (in kJ mol^{-1}) 62

Table 4.3 Changes in Enthalpy for the Phosphorylation of the Various Forms of the Deprotonated Glucose Anion (in kJ mol^{-1}) 64

Table 4.4 Changes in Entropy for the Phosphorylation of the Various Forms of the Deprotonated Glucose Anion (in J mol^{-1} K^{-1}) 66

Table 4.5 Changes in Gibbs Energy for the Phosphorylation of the Various Forms of the Deprotonated Glucose Anion (in kJ mol^{-1}) 67

Table 4.6 Activation Energies (in kJ mol^{-1}) using the HF/6-31G(d) Level of Theory for the Conversion of the Glucose Anion to the Proton Transfer Isomer of the Glucose Anion 73

List of Figures

Figure 1.1 Structure of kanamycin A. 2

Figure 1.2 Structure of the modified kanamycin A antibiotic. 3

Figure 1.3 Modified structure of kanamycin A introducing a fluorine atom and replacing the 3- and 5-hydroxyl groups with hydrogens. 4

Figure 1.4 Structure for gentamicin A. 5

Figure 1.5 Structure for compound 10g. 5

Figure 1.6 Structure of ATP. 7

Figure 1.7 Hydrogen bonding observed between ATP and various residues of *Pf*CKI. 11

Figure 1.8 Two stable conformers of ATP: a) “linear” and b) “chair”. 13

Figure 1.9 The transition state structure for the dephosphorylation of ATP^{4-}. 15

Figure 1.10 The transition state structure for the phosphorylation of deprotonated glucose. 16

Figure 1.11 Reaction coordinate diagram for deprotonated glucose and the deprotonated kanamycin model. 17

Figure 1.12 Reaction coordinate diagram for the dephosphorylation of ATP^{4-} using different basis sets 18

Figure 1.13 The general structure of the derivatives of neutral kanamycin. 19

Figure 1.14 The structures of a) β-D-glucose and b) α-D-glucose. 22

Figure 1.15 Structure of the various conformers of the β anomer of glucose a) GG, b) GT and c) TG. 23

Figure 1.16 a) $^{1}C_{4}$ and b) $^{4}C_{1}$ rotamers of β-D-glucose. 24

Figure 2.1 Chemical structure of the chair conformer of ATP^{4-} with the seven most significant degrees of freedom highlighted in red. 26

Figure 2.2 Structure obtained for the chair conformer of ATP^{4-} run using the HF/6-31G(d) level of theory. 27

Figure 2.3 The resulting structure using the HF/6-31G(d) level of theory from stretching the terminal P-O bond of the linear conformer of $ATP^{4-}\cdot 4H_2O$ to 4.7 Å. 28

Figure 2.4 The fully optimized structure using the HF/6-31G(d) level of theory for the chair conformer of $ADP^{3-}\cdot 2H_2O$. 29

Figure 2.5 The optimized structure of PO_3^- with two water molecules included using the HF/6-31G(d) level of theory. 30

Figure 2.6 The optimized structure for the linear conformer of ADP^{3-} without water added determined using the HF/6-31G(d) level of theory. 31

Figure 2.7 The optimized structure of the phosphorylated glucose anion without water added using the HF/6-31G(d) level of theory. 32

Figure 2.8 The optimized first step transition state structure for the chair conformer using the HF/6-31G(d) level of theory. 33

Figure 2.9 The resulting structure for the second step transition state using the HF/6-31G(d) level of theory keeping the O17-P18 bond length frozen. 34

Figure 3.1 PES scan around the C-C-O-P torsional angle of the chair conformer of ATP^{4-} in increments of 40° from left to right, top to bottom. 35

Figure 3.2 Structure obtained for the proton transfer isomer of ATP^{4-} run using HF/6-31G(d) with four water molecules included. 37

Figure 3.3 IRC for chair $ATP^{4-}\cdot 4H_2O$ using the HF/6-31G(d) level of theory. 42

Figure 3.4 IRC for chairPT $ATP^{4-}\cdot 4H_2O$ using the HF/6-31G(d) level of theory. 42

Figure 3.5 The transition states using the HF/6-31G(d) level of theory for a) chair $ATP^{4-}\cdot 4H_2O$ and b) chair $ATP^{4-}\cdot 5H_2O$. 44

Figure 3.6 Reaction coordinate diagram for the dephosphorylation of chairPT ATP^{4-} using the HF/6-31G(d) level of theory. 47

Figure 3.7 Reaction coordinate diagram for the dephosphorylation of chairPT $ATP^{4-}\cdot 4H_2O$ using the HF/6-31G(d) level of theory. 47

Figure 3.8 Reaction coordinate diagram for the dephosphorylation of both the chair and chairPT isomers of $ATP^{4-}\cdot 4H_2O$ using the HF/6-31G(d) level of theory. 49

Figure 3.9 The transition state structure for the conversion of the chair isomer of ATP^{4-} to the proton transfer isomer of ATP^{4-} without the inclusion of water molecules calculated using the HF/6-31G(d) level of theory. 54

Figure 4.1 The structure obtained using the HF/6-31G(d) level of theory for the TG conformer of the β-D-glucose anion. 57

Figure 4.2 The different isomer obtained from the geometry optimization of the β-L-glucose$\cdot H_2O$ anion using the B3LYP/6-31G(d) level of theory. 60

Figure 4.3 The structure obtained for phosphorylated α-L-glucose·2H_2O anion using the HF/6-31G(d) level of theory. 63

Figure 4.4 The transition state structure for the conversion of the β-D-glucose anion to the proton transfer isomer of the β-D-glucose anion using the HF/6-31G(d) level of theory. 73

List of Schemes

Scheme 1.1 Conversion pathway of PMV to IPP. 9

Scheme 1.2 Propagation of the signal between ATP and pT308. 10

Scheme 4.1 Scheme 4.1 Conversion of D-glucose to L-glucose through L-glucurone. 69

Scheme 4.2 Synthesis of 2,3,4-tri-O-benzyl-1-O-(3-chlorobenozyl)-6-O-(trimethylacetyl)-β-L-glucopyranose from 2,3,4,6-tetra-O-benzyl-D-glucono-1,5-lactone. 71

List of Abbreviations and Symbols

ADP - adenosine diphosphate

APH - aminoglycoside phosphotransferase

ATP - adenosine triphosphate

DFT - density functional theory

DMV - (R)-5-diphosphomevalonate

FIC - fractional inhibitory concentration

HF - Hartree-Fock

IPP - isopentenyl diphosphate

IRC - intrinsic reaction coordinate

MD - molecular dynamics

PES - potential energy surface

*Pf*CKI - *Plasmodium falciparum* casein kinase I

PMK - phosphomevalonate kinase

PMV - (R)-5-phosphomevalonate

pT308 - phosphorylated threonine 308

QM/MM - quantum mechanics/molecular mechanics

rRNA - ribosomal ribonucleic acid

List of Appendices

Appendix I Chair ATP^{4-} PES Scan Energies Using the HF/6-31G(d) Level of Theory (in hartrees) 83

Appendix II Linear ATP^{4-} PES Scan Energies using the HF/6-31G(d) Level of Theory (in hartrees) 85

Appendix III ATP^{4-} Dephosphorylation Data Using the HF/6-31G(d) Level of Theory 87

Appendix IV ATP^{4-} Dephosphorylation Data Using the HF/6-31+G(d) Level of Theory 88

Appendix V ATP^{4-} Dephosphorylation Data Using the B3LYP/6-31G(d) Level of Theory 89

Appendix VI ATP^{4-} Dephosphorylation Data Using the B3LYP/6-31+G(d) Level of Theory 90

Appendix VII Glucose Anion Phosphorylation Data Using the HF/6-31G(d) Level of Theory 91

Appendix VIII Glucose Anion Phosphorylation Data Using the HF/6-31+G(d) Level of Theory 92

Appendix IX Glucose Anion Phosphorylation Data Using the B3LYP/6-31G(d) Level of Theory 93

Appendix X Glucose Anion Phosphorylation Data Using the B3LYP/6-31+G(d) Level of Theory 94

1. Introduction

1.1 Drug-resistant Compounds

Microbes have found ways to render certain drugs ineffective and hence are no longer susceptible to them. Continued misuse of a wide variety of drugs has given rise to organisms being able to resist them, which has led to multidrug resistance. [(1)] An important example is the resistance of staphylococci to penicillin. [(2)]

There are several different types of drug resistance: drug resistance through chromosomal modification, acquired resistance through enzymatic drug modification, altered, substituted and protected drug targets, efflux systems, porins and altered membranes, regulatory genes and single determinants. [(1)]

In a paper by Tenover, three case studies were investigated showing different organisms having drug resistance abilities: *E. coli*., *S. aureus* and *P. aeruginosa*. [(3)] *E. coli* is a common cause of urinary tract infections, with plasmid-encoded β-lactams aiding its resistance. The mechanism studied by Tenover showed that *E. coli* acquired new resistance during infection and that it developed additional resistance to cephamycins. [(3)] *S. aureus* showed reduced susceptibility to vancomycin. The mechanism studied by Tenover showed that the cell wall thickens from accumulation of fragments capable of binding vancomycin extracellularly. [(3)] Okuma et al. showed that *S. aureus* also has developed resistance to oxacillin due to the acquisition of a mobile genetic element containing the *mec*-A resistance gene. [(4)] Tenover showed that *P. aeruginosa* was difficult to control due to the presence of multiple intrinsic and acquired resistance mechanisms: efflux pumps prevent the accumulation of antibacterial drugs by extruding

them before entering the active site while working together with the limited permeability of the outer membrane to produce additional resistance. [3]

There is a need to determine ways to overcome bacterial resistance to drugs. New drugs have since been designed to try and combat these resistance issues to maintain antibiotic efficiency in the future. Kuwahara and Tsuchiya looked at kanamycin A as a potential drug. [5] Kanamycins (the structure of kanamycin A is shown in Figure 1.1) are aminoglycosides having a wide scope of antibacterial activities, but they also have problems: renal toxicity, low transportation into bacterial cells, poor absorption from digestive organs and the resistance developed of bacteria to kanamycins. [5]

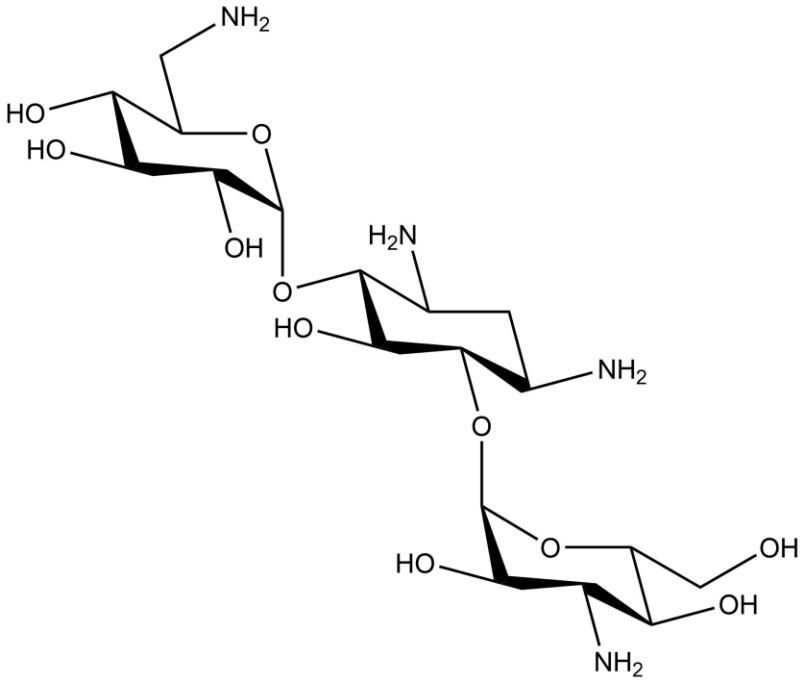

Figure 1.1 Structure of kanamycin A.

Kuwahara and Tsuchiya tried to solve these issues by replacing the hydroxyl groups with fluorine groups to solve the toxicity issue, decreasing the number of substituents to solve the transportation issue and to hinder the acetylation of the NH_2 groups by bacteria

to solve the resistance issue. [5] Thus, they converted the 6-amino-6-deoxy-o-glucose unit to contain solely NH_2 groups (as shown in Figure 1.2). However, it was discovered that the lack of hydroxyl groups produced only slight activity against resistant bacteria and that the replacement of the 6-amino-6-deoxy-o-glucose unit with the 1,4-dioxane framework achieved zero activity against resistant bacteria.

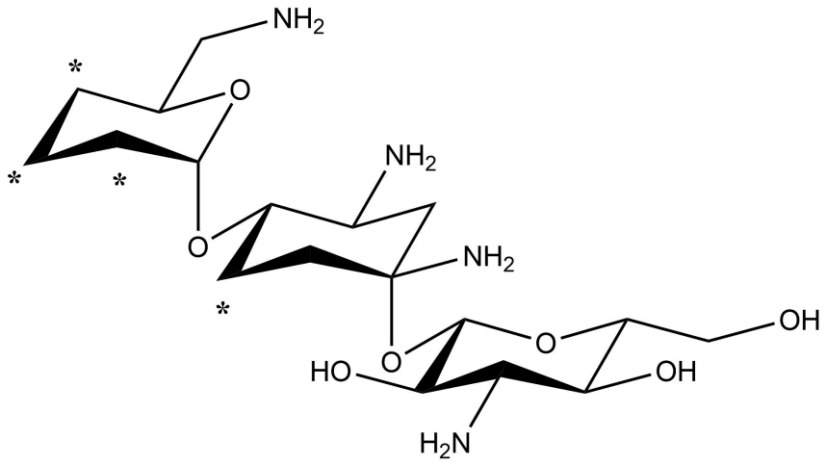

Figure 1.2 Structure of the modified kanamycin A antibiotic. Asterisks indicate the absence of OH groups compare to kanamycin A.

Later, Kobayashi, Ohgami, Ohtsuki and Tsuchiya tried to modify the structure in Figure 1.1 by replacing the 3- and 5-hydroxyl groups with hydrogens. [6] They suggested that the removal of the 3-OH group would prevent 3-phosphorylation by resistant bacteria producing 3-phosphotransferases. The removal of the 5-OH group might ease rotation around the C5-C6 axis, which would allow the NH_2 group to be in a better position to fit bacterial rRNA (ribosomal ribonucleic acid). [7] They also introduced a fluorine atom (which might prevent the production of undesirable 5-o-glycosyl isomers as by-products and favour the formation of 4-o-glycosyl isomers [8]) as shown in Figure 1.3. However, it was determined that this new structure only weakly retained its antibacterial activity.

Kobayashi et al. surmised that this was the result of the steric difference between the pyranose ring in kanamycin A and furanose (which hinders binding of synthetic products to rRNA of bacteria. [6]

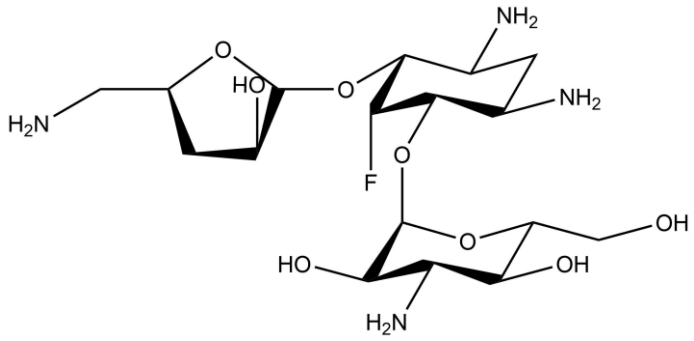

Figure 1.3 Modified structure of kanamycin A introducing a fluorine atom and replacing the 3- and 5-hydroxyl groups with hydrogens.

Azad, Bhunia, Krishna, Shukla and Saxena looked at a novel glycoconjugate of 8-fluoro norfloxacin derivatives and the resistance of *S. aureus* to gentamicin. [9] They stated that the resistance to gentamicin (structure of gentamicin A is shown in Figure 1.4) and its related aminoglycosides results from four mechanisms: reduced uptake due to cell permeability, alterations at ribosomal binding sites, production of aminoglycoside-modifying enzymes and transport defect or membrane impermeabilization. Since the cell membrane of bacteria recognizes carbohydrates, they surmised that cell permeability could be improved by incorporating small ligands. [9] They chose quinolones due to their inherent influence on the area of antimicrobial chemotherapy. They have a wide activity spectrum, high potency, good bioavailability, high serum levels and large volume of distribution resulting in a higher concentration of antibiotic. [9]

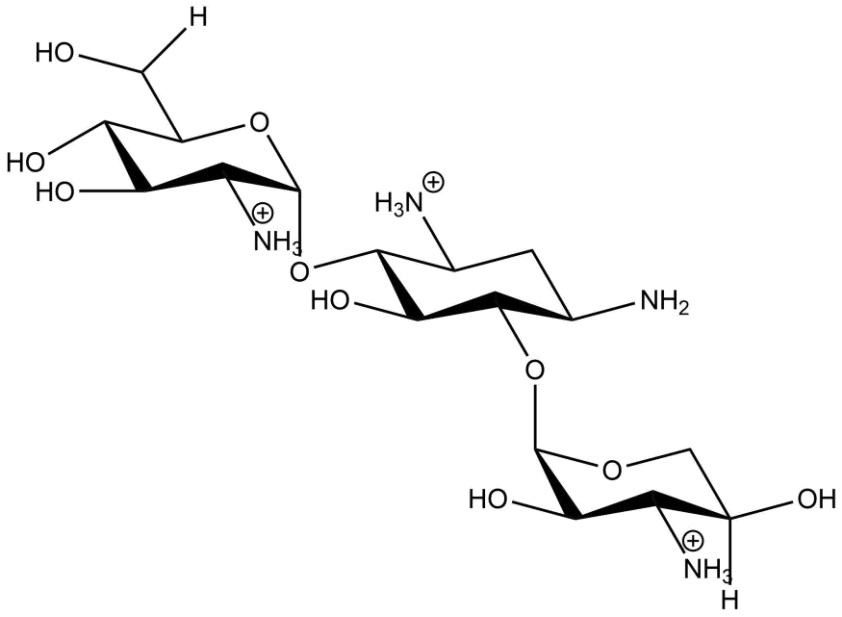

Figure 1.4 Structure for gentamicin A.

In all, eight compounds were synthesized and their activity against *S. aureus* was tested against that of gentamicin. [9] It was discovered that only compound **10g** (Figure 1.5) has a lower minimum inhibitory concentration in some cases compared to using gentamicin and that most compounds only performed better than gentamicin when used against gentamicin resistant *S. aureus*.

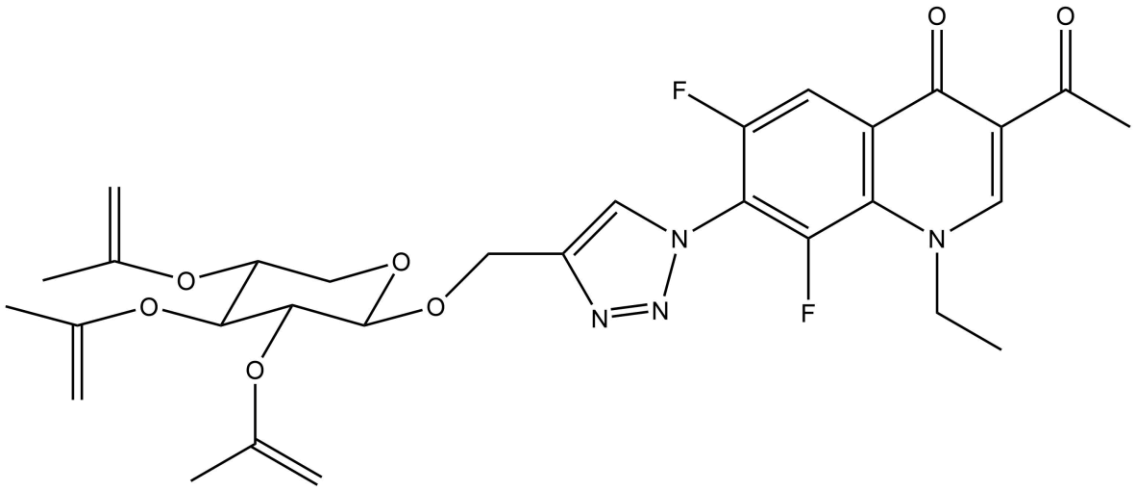

Figure 1.5 Structure for compound **10g**.

Amani, Barjini, Moghaddam and Asadi looked at the *in vitro* synergic effect, which is achieved by combining two antimicrobial drugs eliciting an additive effect, using the CM11 peptide when used with other antibiotics against six multidrug resistant bacteria. [10] They proposed that the dose of an antibiotic in treatment of drug resistant bacteria could be significantly reduced if used in combination with the CM11 peptide, which would enable the use of a lower concentration of antibiotic and potentially restore the effectiveness of an antibiotic. The best results for the CM11 peptide were obtained when used in combination with ceftazidime against *P. aeurginosa* and when used in combination with penicillin against *S. aureus*. However, no effect was observed when the CM11 peptide was used in combination with gentamicin against *P. aeruginosa* or *K. pneumoniae*, or when it was used in combination with ampicillin against *A. baumannii*, *K. pneumoniae* or *S. typhimurium* or when it was used in combination with amikacin against *P. aeruginosa*.

1.2. ATP Phosphorylation

One way to solve the issue of multidrug resistance is by looking at the mechanism of phosphorylation using adenosine triphosphate (ATP) (structure is shown in Figure 1.6) as the phosphate donor. Phosphorylation of antibiotics could potentially lead to a change in conformation or a change in environment before reaching the active site of rRNA of bacterial cells. If the phosphorylation of antibiotics can be prevented from occurring, then they would retain their antibacterial activity and thus help solve the issue of drug modification by bacteria. [(1)]

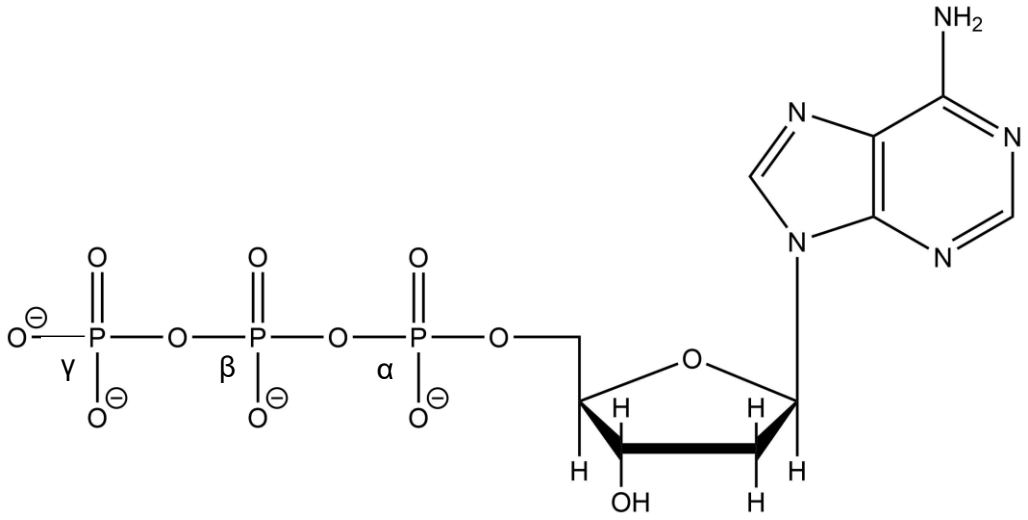

Figure 1.6 Structure of ATP. Phosphorus atoms are labelled with Greek letters.

There have been several previous studies concerning the mechanism involving phosphorylation using ATP as the phosphate donor. In a paper by Huang et al., the phosphorylation mechanism of phosphomevalonate kinase was studied using ATP. [(11)] The first topic investigated in their paper was the identification of key residues in the catalytic reaction pathway. They determined that phosphomevalonate kinase (PMK) transfers the γ-phosphoryl group of ATP to the phosphoryl group of (R)-5-

phosphomevalonate (PMV) yielding (R)-5-diphosphomevalonate (DMV), which can be converted to isopentenyl diphosphate (IPP) (the reactions are shown in Scheme 1.1). The crystal structure showed that a Mg^{2+} ion is coordinated to the γ-phosphoryl group in ATP and to the phosphoryl group of the substrate. It was observed that Lys9 forms strong ionic interactions with the phosphoryl group of PMV and with the γ-phosphoryl group of ATP, which helps to stabilize both the substrate and the nucleotide along the reaction pathway. They also determined that PMK helps catalyze the transfer of the γ-phosphate of ATP to another negatively charged phosphate in the substrate. They also discovered that human galactokinase follows a direct phosphorylation mechanism, in which Arg228 helps stabilize the negative charge developed at the β-, γ-bridging oxygen atom of ATP during bond cleavage. It was also found that Mg^{2+} is octahedrally coordinated to Asp297, the phosphoryl group of PMV, the γ-phosphoryl group of ATP and three water molecules; Lys9 is located between PMV and ATP which helps to stabilize both the γ-phosphoryl group of ATP and the phosphoryl group of PMV.

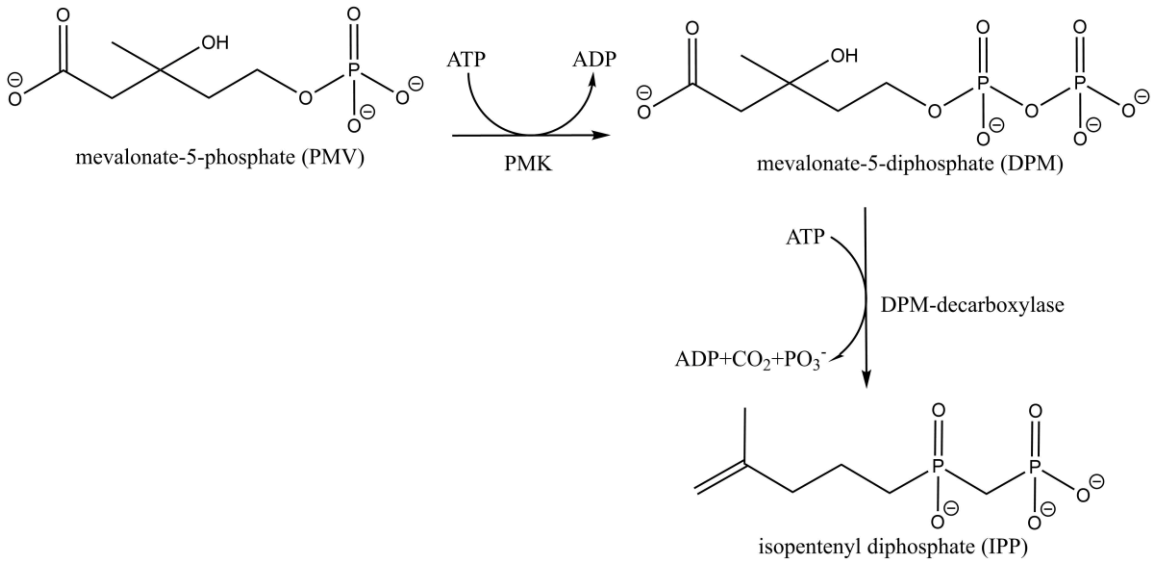

Scheme 1.1 Conversion pathway of PMV to IPP. (Adapted with permission from reference 11. Copyright 2018 American Chemical Society)

The second topic that was studied by Huang et al. was the effect of sequence alterations on Mg^{2+} coordination. [11] They discovered that switching Lys9 to arginine resulted in distortion of Mg^{2+} coordination, the loss of one water molecule and destabilization of the active site; all of which suggests that lysine helps orient and facilitate phosphate transfer. Switching Lys9 for methionine also resulted in the loss of one water molecule and the formation of an unstable pentacoordinate Mg^{2+} complex, which suggests that lysine helps proton transfer during phosphorylation.

The last topic studied by Huang et al. was the study of the reaction pathway of PMK (shown in Scheme 1.1) by QM/MM calculations. [11] They proposed that the tight hydrogen bond network would facilitate proton transfer from the hydroxyl group of the substrate to the γ-phosphoryl group of ATP. They proposed that Lys9 helps stabilize the transition state and the phosphorylated product, while Lys101 helps neutralize the negative charge at the β-, γ-bridging oxygen atom of ATP during phosphorylation.

In a paper by Lu et al., the mechanism of ATP-dependent allosteric protection of protein kinase B phosphorylation was studied. [12] They looked at the molecular basis of the allosteric communication from ATP to phosphorylated threonine 308 (pT308). They discovered that four residues, Thr160, Phe161, Glu161 and His194 were involved in propagating the signal from ATP to pT308 (shown in Scheme 1.2). It was hypothesized that the alteration of residues could disrupt propagation and it was later discovered that the H194A mutant abolished the ATP-dependent resistance to phosphorylation. [12]

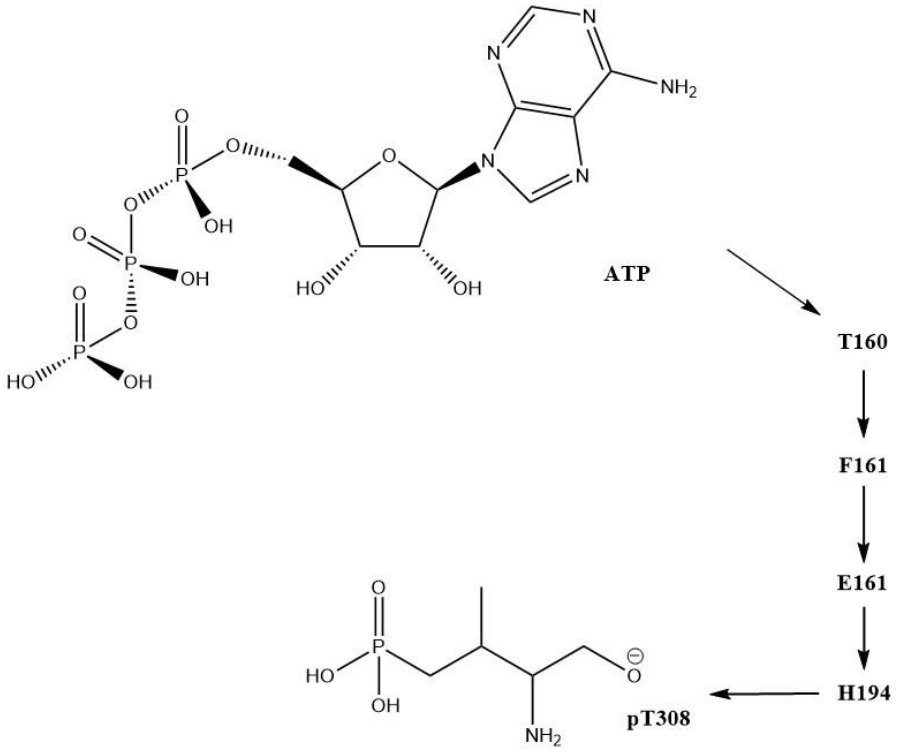

Scheme 1.2 Propagation of the signal between ATP and pT308.

A paper by Dehury, Behera and Mahapatra looked at the structural dynamics of casein kinase I from malarial parasite *Plasmodium falciparum* (*Pf*CKI) with insights from theoretical modelling and molecular simulations. [13] They performed a trajectory analysis in which the ATP-binding cleft showed comparatively higher fluctuation along with the

important loops. An inconsistent hydrogen bonding pattern of ATP was observed with Asp132, Leu85, Asp83 and Ser19 which Dehury et al. proposed could be due to the dynamic behaviour of the important regulatory loops, the ATP binding motif and slight movement of the ligand within the pocket. [13] Hydrogen bonds were also observed between ATP and the atoms of Phe150, Gly151, Ser17 and Ser88 of *Pf*CKI. The various hydrogen bonds observed are shown in Figure 1.7.

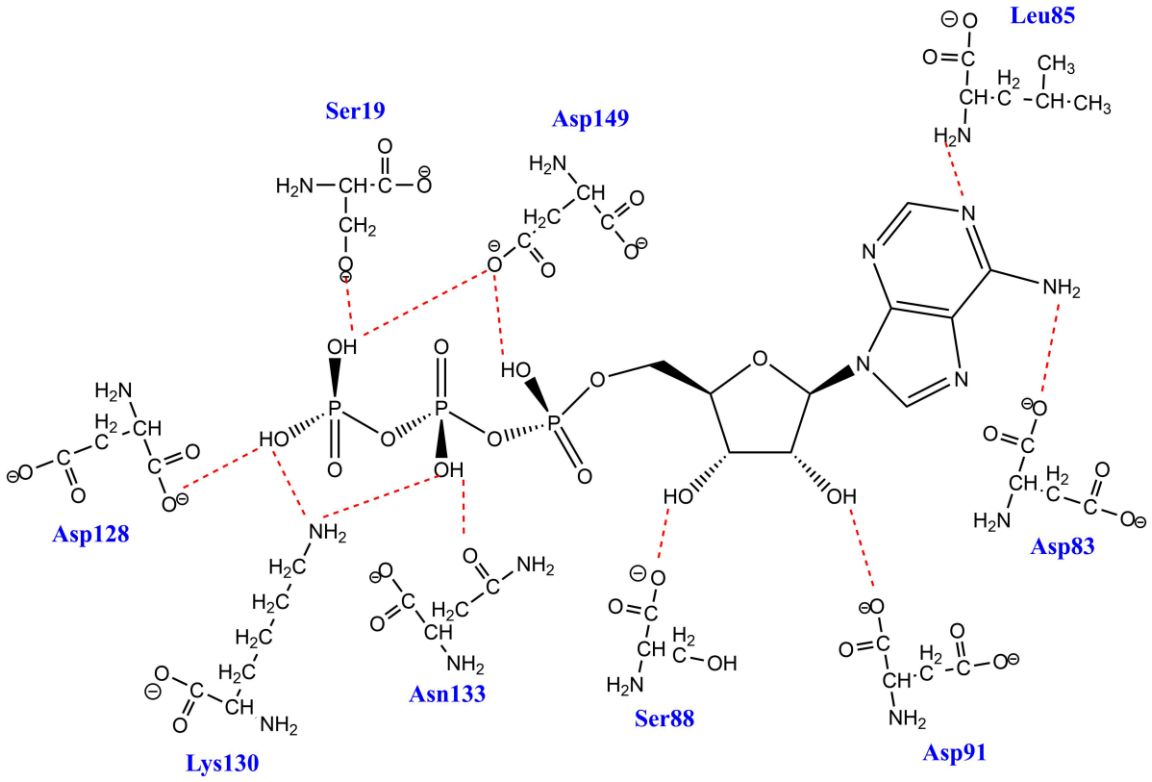

Figure 1.7 Hydrogen bonding observed between ATP and various residues of *Pf*CKI. Hydrogen bonds are shown in red dashed lines. (Adapted from reference 13. Copyright 2018 Elsevier)

Dehury et al. also performed molecular dynamics (MD) simulations. [13] After MD simulations, the orientation of ATP changed whereby the γ-phosphate group moved away from the core cavity. The hydrogen bond between the nitrogen atom of Ser19 with ATP was broken during the MD simulation whereas the electrostatic interaction between

Lys38 with ATP was conserved throughout the MD simulation. The binding pocket of ATP was discovered to be composed of both polar and hydrophobic residues, providing an ideal cavity to hold the ligand and the active site. The conserved residues formed a tight network of hydrophobic environment to anchor the ligand, which allowed for the compensation of the loss of hydrogen bonding. [13]

1.3 Conformers of ATP

The fully deprotonated form of ATP can take on two different conformers [14-18] that are stabilized by hydrogen bonding as shown in Figure 1.8: a) a conformation that has hydrogen bonding between the hydrogen of ribose and the closest phosphoryl group of the chain to the ribose, which will be called “linear” from this point forward and b) a conformation that has hydrogen bonding between the hydrogen of ribose and the middle phosphoryl group of the chain, which will be termed “chair” from this point forward.

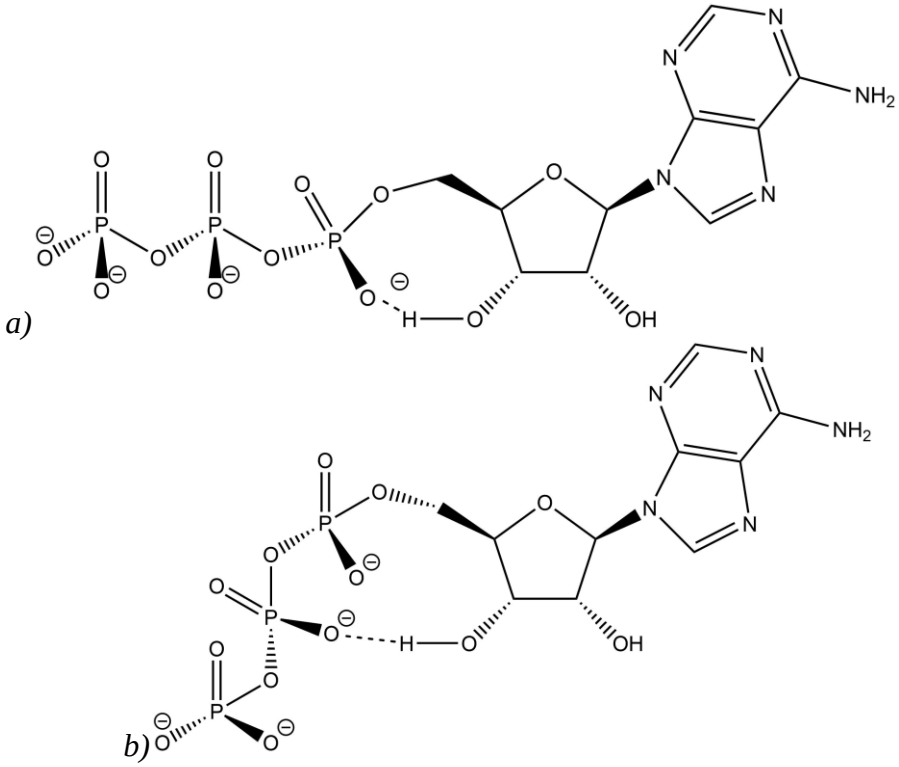

Figure 1.8 Two stable conformers of ATP^{4-}: a) “linear” and b) “chair”. Hydrogen bonding is indicated with a dashed line between the O and H atoms.

There have been many ATP^{2-} conformer studies done in which only the terminal phosphate has negative charges. Burke, Pearce, Boxford, Bruckmann and Dessent looked at the intramolecular stabilization of ATP^{2-} in the gas phase using mass spectrometry. [14]

Wang, Izatt, Oscarson and Gillespie did a ^{1}H-NMR study of the interaction of ATP^{2-} with protons and Mg^{2+}. [15] Miyazaki et al. looked at the conformation of aqueous disodium ATP^{2-} solution using X-ray diffraction. [16] There have also been studies of ATP^{2-} as part of coordination with Mg^{2+}, in motor proteins in which it was determined that ATP takes on a more compact structure, [17] and in anthrax edema factor (which is a mode of virulence of anthrax upon infecting host cells), in which it was discovered that the phosphate tail is in a more stretched configuration with hydrogen bonding between the sugar and phosphorus atom α in Figure 1.6 [18]. However, under normal conditions in the body, ATP is in the fully deprotonated form (ATP^{4-}) [19], in which there is no computational data available concerning its conformers. Results for phosphorylation using ATP^{4-} would be significantly different if the most stable conformer of ATP^{4-} was not being used. To ensure that the lowest energy conformer of ATP^{4-} was being used for this project, it was decided to do a conformational analysis on ATP^{4-}.

1.4 Kanamycin Studies

1.4.1 Glucose, Neutral Kanamycin and a Simplified Model of Kanamycin

The first three compounds studied for their reactions with ATP were glucose, neutral kanamycin and a simplified model of kanamycin in which one D-(+)-glucosamine group is used instead of three. [20] All these compounds were deprotonated and then reacted with ATP both in the gas phase and with water included. Initially, the oxygen linker atom of ATP was 1.7 Å from the terminal phosphorus atom (this bond is shown in Figure 1.9). Upon arrival at the first transition state, the distance of the oxygen linker atom of ATP from the terminal phosphorus atom increased to 2.9 Å. This suggests that the bond between PO_3^- and ADP^{3-} is breaking. The intermediate occurs after this bond has been broken to give ADP^{3-} and PO_3^-.

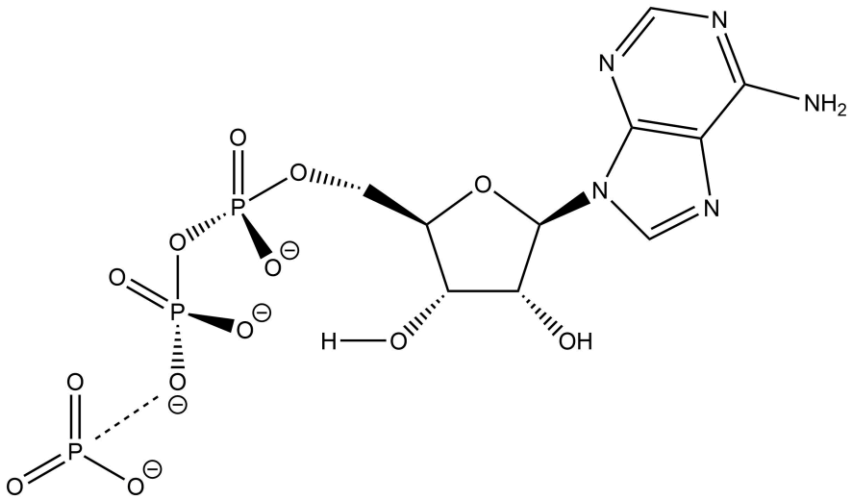

Figure 1.9 The transition state structure for the dephosphorylation of ATP^{4-}. The P-O bond between ADP^{3-} and PO_3^- is shown as a dashed line.

A second transition state was reached where the distance between the oxygen atom of the sugar and the phosphorus atom of PO_3^- was decreased to 3.5 Å (this bond is shown in Figure 1.10). This suggests possible bond formation between the oxygen atom of the

sugar and the phosphorus atom of PO_3^-. The final products were achieved with a final distance between the oxygen atom of the sugar and the phosphorus atom of PO_3^- being 1.7 Å, the same as the initial distance between the phosphorus and oxygen atoms on ATP, thus suggesting the bond was indeed formed.

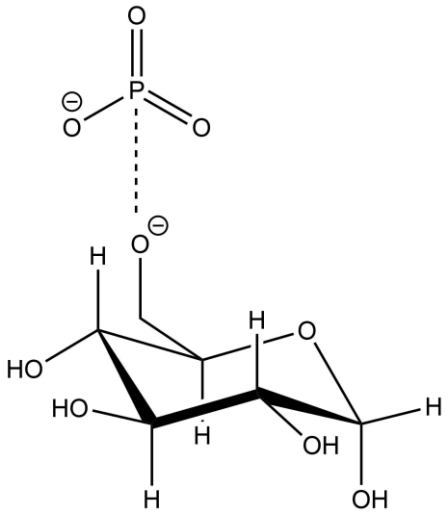

Figure 1.10 The transition state structure for the phosphorylation of deprotonated glucose. The P-O bond between glucose and PO_3^- is shown as a dashed line.

The reaction coordinate diagrams for the reaction between ATP^{4-} and either glucose or the kanamycin model are shown in Figure 1.11.

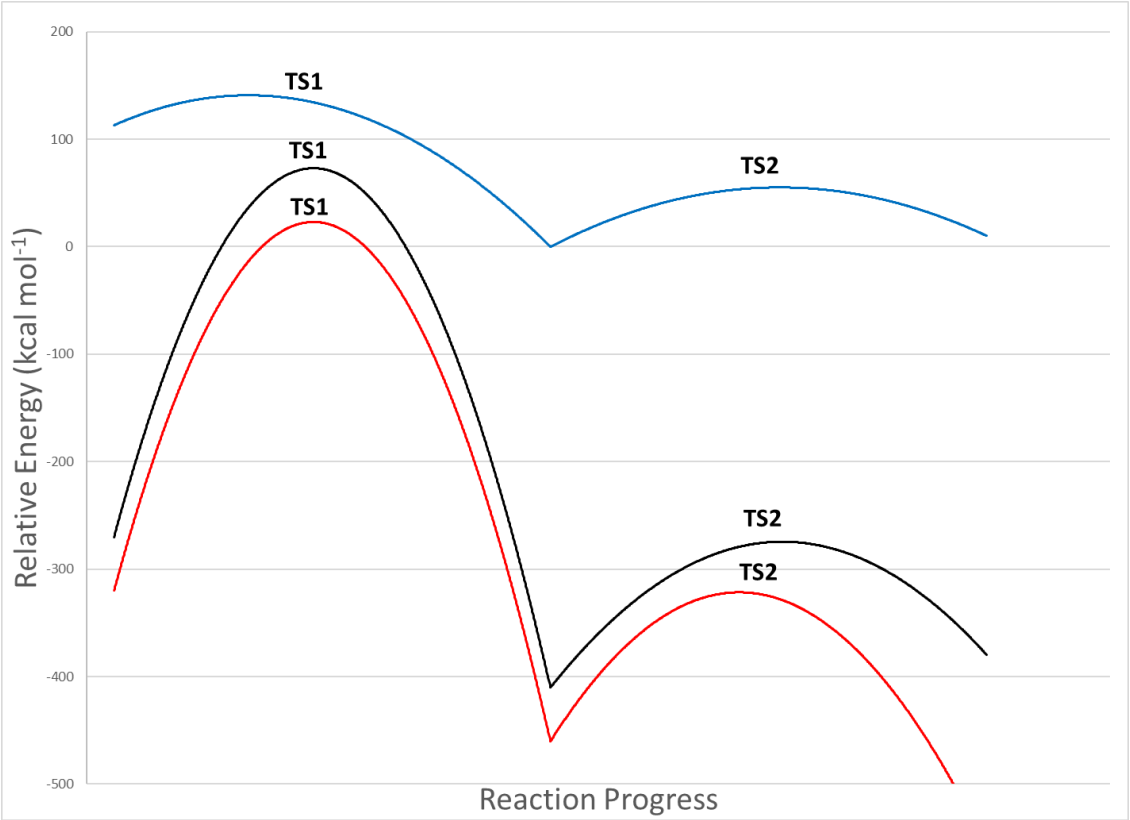

Figure 1.11 Reaction coordinate diagram for deprotonated glucose and the deprotonated kanamycin model. Glucose without water included is in red; kanamycin model is in black and glucose with water is in blue. The upper line for each compound is the dephosphorylation of ATP^{4-} while the lower line for each compound is the phosphorylation of each compound. (Data in figure used with permission from reference 20)

Different basis sets were also used in determining the thermochemistry of reactions of ATP with glucose, neutral kanamycin and the kanamycin model: STO-3G, 3-21G and 6-31G. [20] The reaction coordinate diagrams were plotted using the above basis sets shown in Figure 1.12. It was determined that the energy of ATP^{4-} was highest using the 3-21G basis set and lowest using the 6-31G basis set. The activation energy was largest using 6-31G and smallest using STO-3G. The energies of the products (ADP^{3-} and PO_3^-) were roughly the same using all three basis sets, therefore the ΔE was largest using the 3-21G basis set and smallest using the 6-31G basis set.

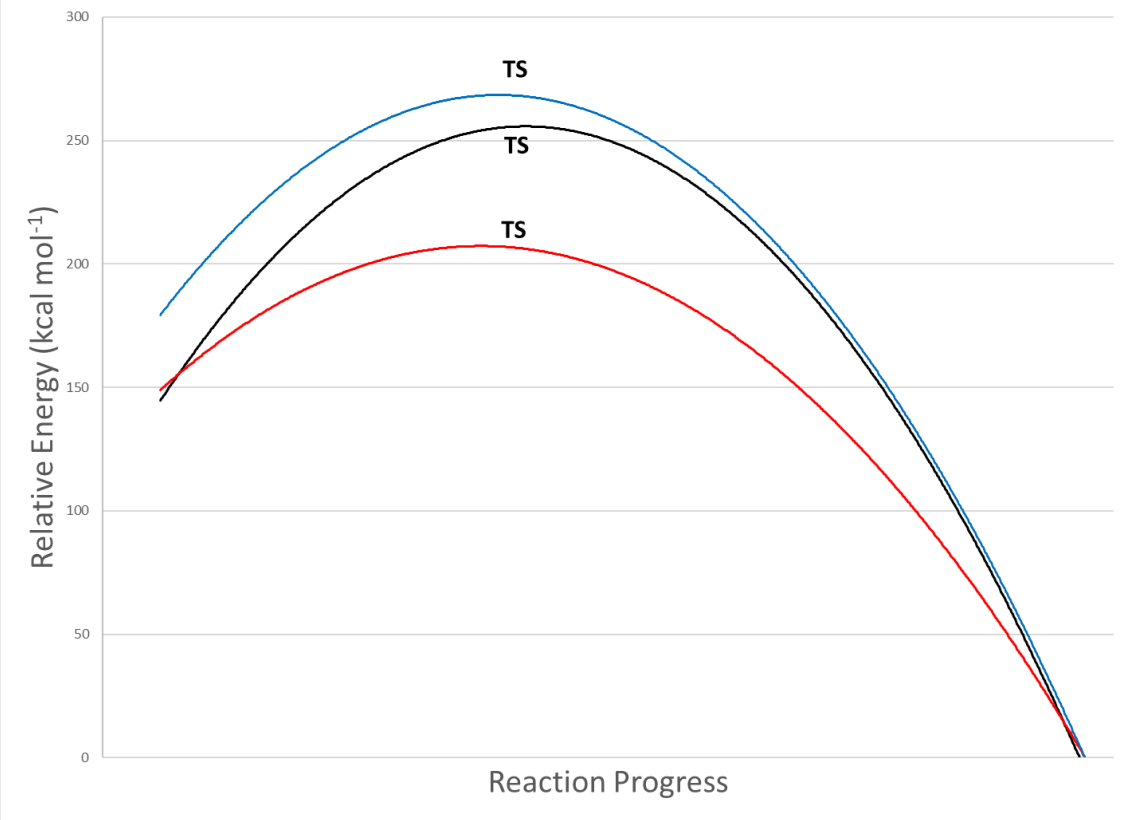

Figure 1.12 Reaction coordinate diagram for the dephosphorylation of ATP^{4-} using different basis sets. Red = STO-3G, blue = 3-21G and black = 6-31G. (Data in figure used with permission from reference 20)

1.4.2 Variations of Neutral Kanamycin

The next three compounds studied were variations of neutral kanamycin in which some of the functional groups on the rings were changed: kanamycin A, kanamycin 3'RGK and kanamycin 3'RGH. [21] The general structure of these derivatives is shown in Figure 1.13. Kanamycin A has hydroxyl groups at the R1 and R2 positions and hydrogens at the R3 and R4 positions. Kanamycin 3'RGK has hydrogen at the R1, R3 and R4 positions with the amino acid chain Arg-Gly-Lys-Gly attached to the R2 position. Kanamycin 3'RGH is like kanamycin 3'RGK except that the terminal $CH_3(CH_2)_2NH_2$ group of lysine is replaced with imidazole.

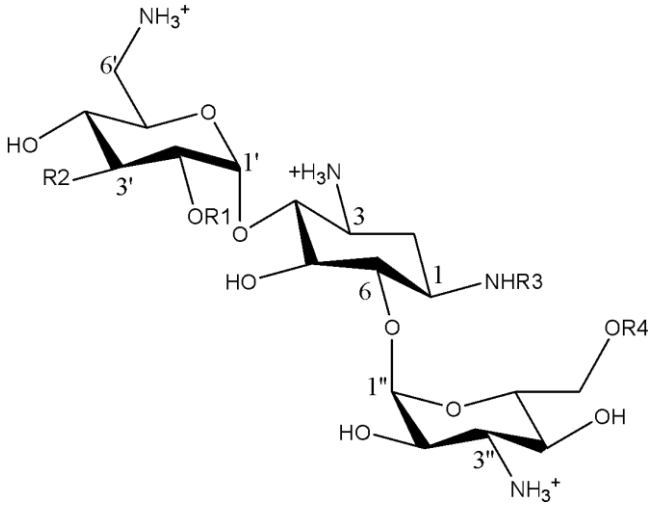

Figure 1.13 The general structure of the derivatives of neutral kanamycin.

For each of the four derivatives, their reactions with either a) APH, ADP, Mg^{2+} and water and/or b) bacterial rRNA were studied. [21] The docking score for each reaction, which is the number of favorable interactions such as hydrogen bonds or hydrophobic contacts (calculated using equation 1.1 where vdW is the van der Waals energy, Coul is the Coulombic energy, Lipo is the lipophilic term derived from hydrophobic grid potential, H Bond is the hydrogen bonding term, Metal is the metal binding term, Rewards are the rewards and penalties that cover other terms than those mentioned like buried polar groups, hydrophobic enclosure, amide twists etc., Rot B is the penalty for freezing rotatable bonds and Site is the polar but non-hydrogen bonding interactions in the active site [22]), and their binding energies are listed in Table 1.1.

Docking Score = 0.05 vdW + 0.15 Coul + Lipo + H Bond + Metal + Rewards + Rot B + Site (1.1)

For both the docking score and the binding energy, a more negative value indicates that the interaction is favoured and binding is more likely to occur. The most negative docking scores were observed for kanamycin 3'RGK. For the reaction with APH, ADP,

Mg^{2+} and water, the most negative binding energy was observed for kanamycin 3'RGK. For the reaction with bacterial rRNA, the most negative docking score was observed for kanamycin 3'RGH. [21]

Table 1.1 Docking Scores and Binding Energies for the Reactions of Kanamycin Derivatives with a) APH, ADP, Mg^{2+} and water and b) bacterial rRNA (Data used with permission from reference 21)

Kanamycin Derivative	**Docking Score**	**Binding Energy (kJ mol^{-1})**
Kanamycin A	a) -6.03 b) -5.95	a) -241.5 b) -280.0
Kanamycin 3'RGK	a) -8.88 b) -9.16	a) -505.7 b) -176.1
Kanamycin 3'RGH	a) -5.48 b) -8.39	a) -436.7 b) -389.6

There are also newer APH linkers that have been developed, with some of them, conjugate 3b, showing better promise than the previously modified versions of neutral kanamycin. [21] The binding energies and docking scores for the best three docking poses (defined as having the least negative docking scores) of the linkers, as given in Table 1.2, are lower than the previous kanamycin derivatives, so they would be less susceptible to being phosphorylated. In addition, the zone of inhibition (the diameter that is saturated by an antimicrobial agent) is higher for the new linkers when compared to kanamycin, as shown in Table 1.3. [21] We are awaiting the patents for these compounds, so no structures for these linkers can be shown at this time.

Table 1.2 Docking Scores and Binding Energies for the Best Three Docking Poses of Kanamycin and Conjugate 3b with a) APH, ADP, Mg^{2+} and water and b) bacterial rRNA (Data used with permission from reference 21)

Compound	**Docking Score**	**Binding Energy (kJ mol^{-1})**
Kanamycin	a) -6.64, -6.53, -6.21 b) -6.91, -6.43, -6.04	a) -376.3, -306.5, -294.3 b) -296.3, -246.9, -232.0
Conjugate 3b	a) -6.10, -6.03, -6.02 b) -6.61, -6.57, -6.45	a) -256.6, -219.9, -220.1 b) -55.7, -66.0, -39.2

Table 1.3 Zone of Inhibition of Kanamycin and Conjugate 3b Against Various Pathogenic Bacteria (Data used with permission from reference 21)

Compound	**Zone of Inhibition (mm) Against Various Pathogenic Bacteria**					
	E. Coli. MC 4100	*E. Coli. DH 5α*	*Staphylococcus aureus*	*Streptococcus pyogenes*	*Listeria monocytogenes*	*Bacillus Subtilis*
Kanamycin	29	28	33	31	27	32
Conjugate 3b	41	32	36	39	38	37

1.5 Conformations of Glucose

Unlike those of ATP^{4-}, the various conformations of glucose have been previously studied using *ab initio* calculations in the gas phase and in solution. It has been shown experimentally that the β anomer of glucose, shown in Figure 1.14a, is more stable than the α anomer, shown in Figure 1.14b. [23]

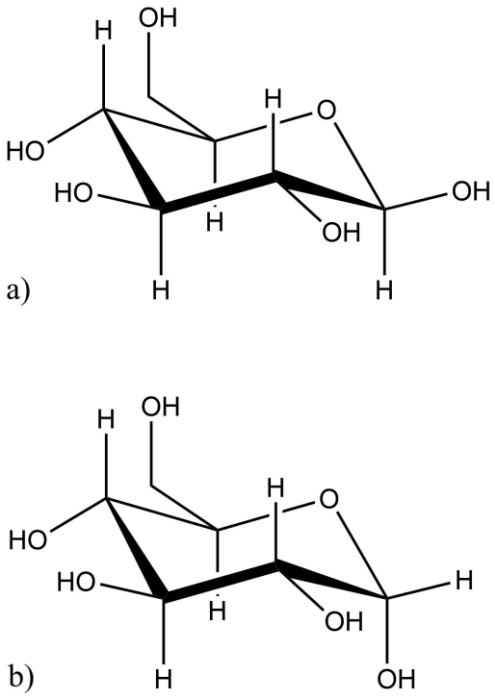

Figure 1.14. The structures of a) β-D-glucose and b) α-D-glucose.

The C6-O6 bond can be oriented in three possible positions (see Figure 1.15 for the various conformations of the β anomer): 1) *gauche* to both C_5-O_5 and C_5-C_4 bonds (GG, Figure 1.15a), 2) *gauche* to the C_5-O_5 bond and *trans* to the C_5-C_4 bond (GT, Figure 1.15b) and 3) *trans* to the C_5-O_5 bond and *gauche* to the C_5-C4 bond (TG, Figure 1.15c). [23] In aqueous solutions, it has been shown by Ha et al. using MD simulations that both the GG and GT conformers are prevalent, and that the TG conformer is more favored in

the gas phase. [24] Studies on glucose crystals have shown that glucose is in the GT conformer for the α anomer and is in the GG conformer for the β anomer. [25]

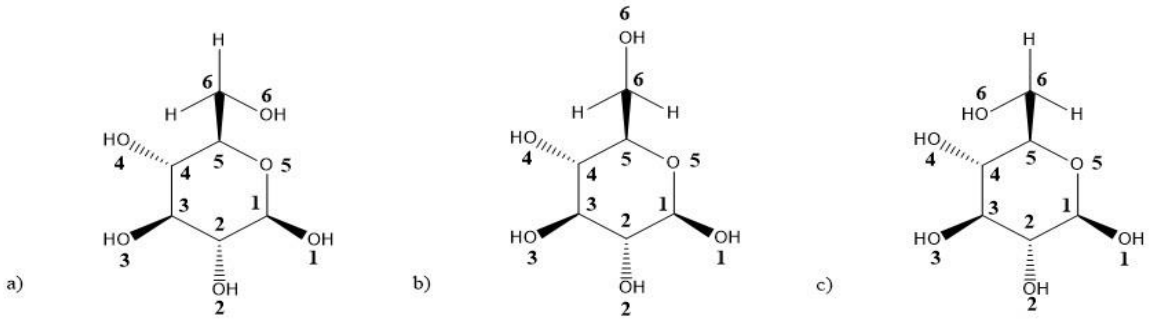

Figure 1.15 Structure of the various conformers of the β anomer of glucose a) GG, b) GT and c) TG.

Polavarapu and Ewig showed that by using the 4-31G basis set, the GG, G1 conformer of the α anomer was most stable using *ab initio* calculations. [23] However, upon switching to the 6-31G(d) basis set, the energy difference between the α and β anomers decreased. They suggested that the β anomer might be more stable using larger basis sets. [23]

Csonka, Éliás and Csizmadia explored the relative stability of the $^{1}C_{4}$ (which has all substituents in an axial position) and $^{4}C_{1}$ (which has all substituent in an equatorial position and is the favoured conformation) chair forms of β-D-glucose (as shown in Figure 1.16) using different density functional theory (DFT) methods. [26] Experimentally, Csonka et al. showed that the G+ rotamer is more stable than the T rotamer, however they only observed this to be the case using the B3P/aug-cc-pVDZ//MP2/cc-pVDZ level of theory. [26] NMR experiments show that the G- rotamer of the $^{4}C_{1}$ conformer is slightly more populated than the G+ rotamer while the T rotamer is barely populated. [27] Studies done on glucose crystals showed that the G- rotamer is found for the $^{4}C_{1}$ conformer of α-D-glucose. [28]

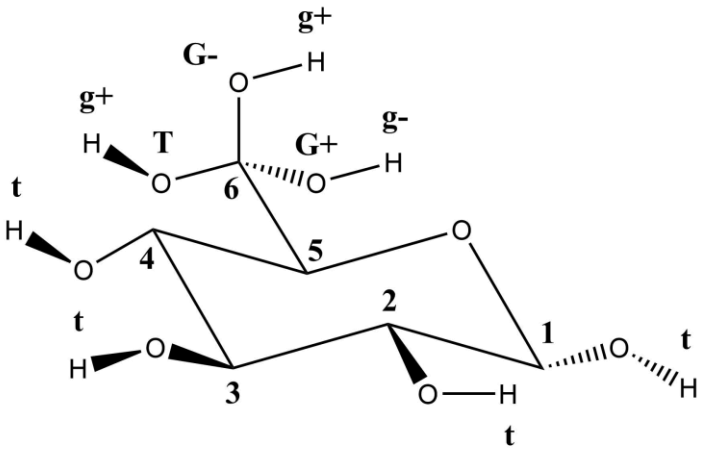

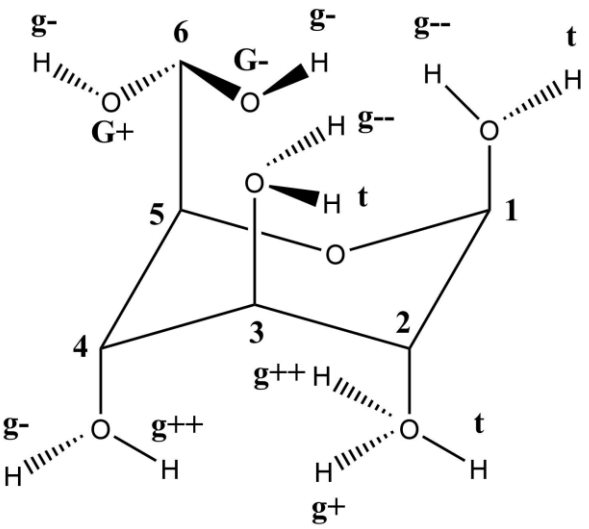

Figure 1.16 a) $^{4}C_{1}$ and b) $^{1}C_{4}$ rotamers of β-D-glucose. The idealized C(n + 1)-C(n)-O-H torsions are denoted by G+ (*gauche* clockwise (60°)), T (*anti* (180°)) and G- (*gauche* counterclockwise (-60°)) where n = 1, 2, 3, or 4; g++ or g-- notate torsions far from the idealized values. (Adapted from reference 26. Copyright 2018 Elsevier)

Csonka et al. reasoned that the Hartree-Fock (HF) method in conjunction with good basis sets tend to underestimate the H---OH interactions due to over-concentration of electron density around atoms in covalent bonding regions whereas it is under-concentrated in other regions. This is important for $^{1}C_{4}$ conformers due to the ease in decrease of 1-3 O-H interactions. Therefore, a double zeta basis set would be needed for

an optimal choice using the HF method. [26] They also state that the inclusion of electron correlation using either MP2 or CCSD methods leads to large differences in energy between the two conformers, which is due to increased stabilization of the H---OH interaction in the ring of the $^{1}C_{4}$ conformations. Therefore, larger basis sets using MP2 or CCSD methods would be needed to come reasonably close to the experimental results. [26]

Finally, they mention that, while DFT methods using double zeta basis sets experience the same problem as using the MP2 method, the addition of diffuse functions decreased the error relative to experimental results. It was argued that this was due to the long-range portion of the correlation and exchange functionals helping to describe OH---O interactions more accurately with the increase in space for the electrons from the nuclei. [26]

Based upon all the previous glucose conformational studies, it was decided to use the conformation having the hydroxymethyl group *gauche* to both the C-O and the C-C bonds of the ring nearest to the hydroxymethyl group using the $^{4}C_{1}$ chair conformer of β-D-glucose.

2. Methods

2.1 ATP and Glucose Conformers

The initial structures for both the linear and chair conformations of ATP^{4-} as well as the deprotonated form of the lowest energy conformer of glucose previously reported [23,26] were built using WebMO [29] and run on Gaussian 09 [30] both without water (ATP^{4-}) and with water molecules included ($ATP^{4-}\cdot nH_2O$, where *n* is the number of water molecules) using the HF [31]/6-31G(d) level of theory with geometry optimization and frequency calculations. Four water molecules for ATP^{4-} and one water molecule for the glucose anion were initially included to stabilize the negative charges.

To ensure that the structures obtained were indeed the lowest in energy, the resulting structures obtained for both linear and chair ATP^{4-} were analyzed by doing a PES scan around each of the seven most significant degrees of freedom as shown in red in Figure 2.1. Each of the torsional angles were rotated by 10 degrees while allowing the rest of the molecule to relax into its lowest energy geometry at each point.

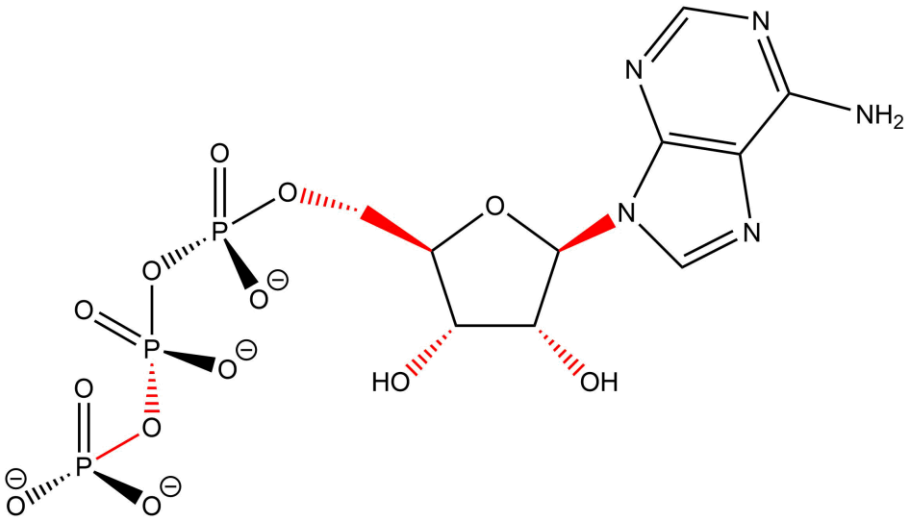

Figure 2.1 Chemical structure of the chair conformer of ATP^{4-} with the seven most significant degrees of freedom highlighted in red.

The resulting structures for ATP^{4-} (an example is shown in Figure 2.2) and the glucose anion were then used as starting points to run geometry optimizations and vibrational frequency calculations on Gaussian 09 using the HF/6-31+G(d), B3LYP [32]/6-31G(d) and B3LYP/6-31+G(d) levels of theory. All optimized structures for this project shown were visualized using Jmol [33].

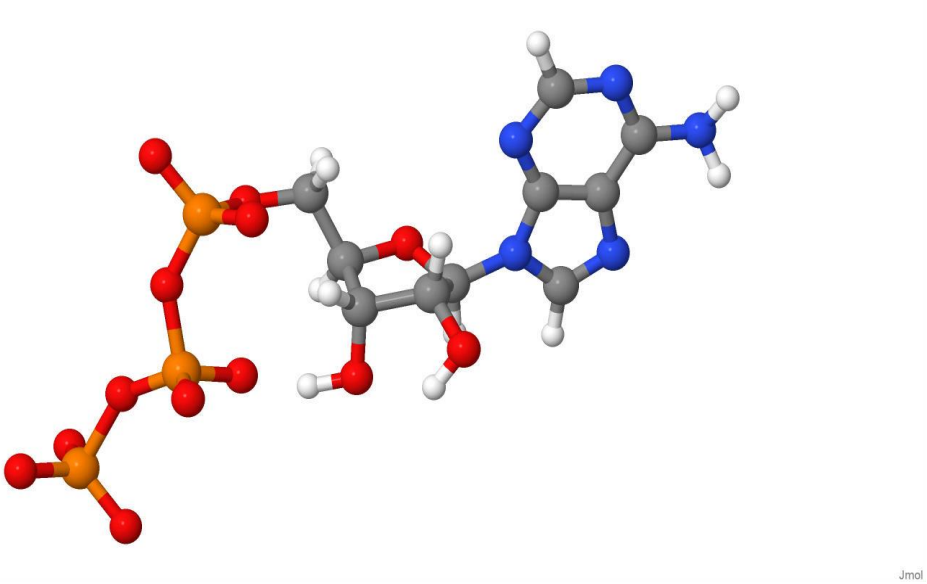

Figure 2.2 Structure obtained for the chair conformer of ATP^{4-} run using the HF/6-31G(d) level of theory.

2.2 Phosphorylation Reaction Products

Geometry optimizations of ADP^{3-} with water and PO_3^- for both the chair and linear conformers using HF/6-31G(d) were obtained by increasing the terminal P-O bond distance of ADP^{3-} with water by 0.5 Å up to a terminal distance of around 4.7 Å, which pulls the PO_3^- to an optimal distance as previously reported [20] (an example of the linear conformer structure is shown in Figure 2.3).

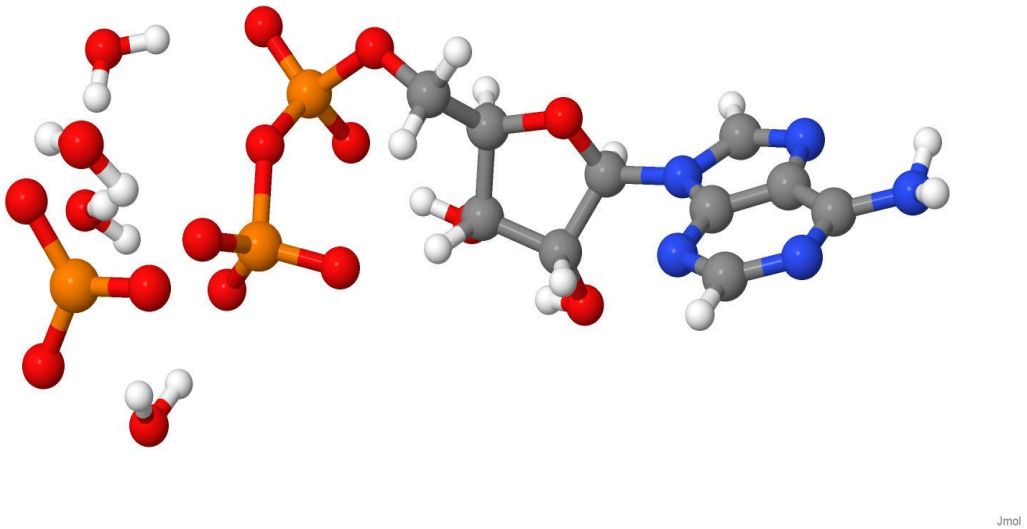

Figure 2.3 The resulting structure using the HF/6-31G(d) level of theory from stretching the terminal P-O bond of the linear conformer of $ATP^{4-}\cdot 4H_2O$ to 4.7 Å.

PO_3^- and either one water molecule (for the linear conformer) or two water molecules (for the chair conformer) were then removed from the resulting structures (according to the number of water molecules pulled away with PO_3^- during the separation of PO_3^- from ADP^{3-}). The remaining structures were re-optimized (the fully optimized structure for the chair conformer is shown in Figure 2.4) using HF/6-31G(d) to give ADP^{3-} with water molecules included ($ADP^{3-}\cdot nH_2O$ where *n* is the number of water molecules). The resulting structures were then used as a starting point to calculate the geometries and

vibrational frequencies using the HF/6-31+G(d), B3LYP/6-31G(d) and B3LYP/6-31+G(d) levels of theory.

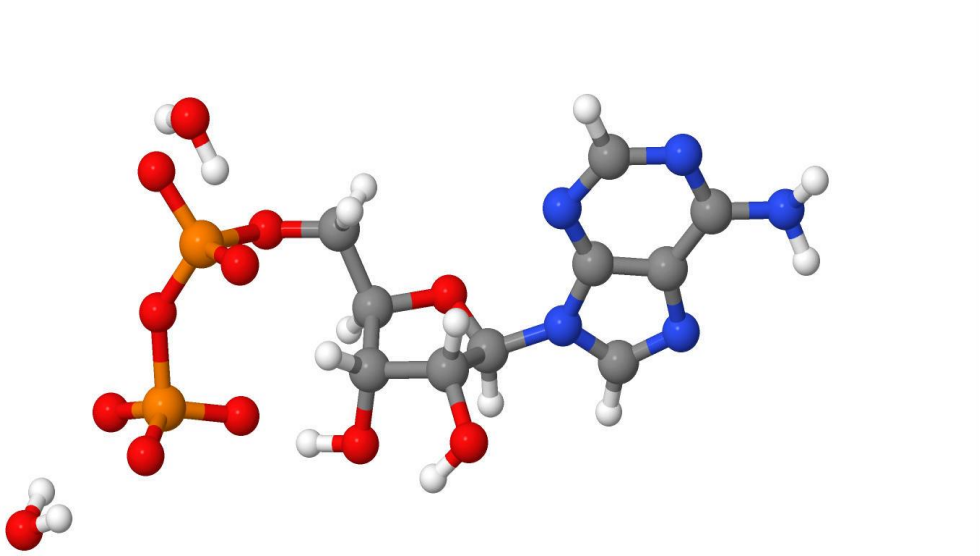

Figure 2.4 The fully optimized structure using the HF/6-31G(d) level of theory for the chair conformer of $ADP^{3-}\cdot 2H_2O$.

The geometries and vibrational frequencies of PO_3^- with either one water molecule (for the linear conformer of ADP^{3-}) or two water molecules (for the chair conformer of ADP^{3-}, the fully optimized structure is shown in Figure 2.5) were also calculated using HF/6-31G(d). The resulting structures were then used to determine the geometries and vibrational frequencies using HF/6-31+G(d), B3LYP/6-31G(d) and B3LYP/6-31+G(d) levels of theory.

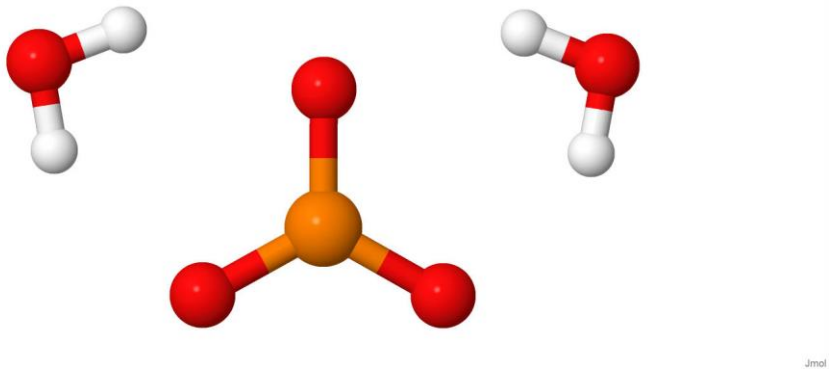

Figure 2.5 The optimized structure of PO_3^- with two water molecules included using the HF/6-31G(d) level of theory.

The ADP^{3-} product without water for both the chair and linear conformers (an example of the linear conformer structure is shown in Figure 2.6) were then obtained using HF/6-31G(d) by removing either two water molecules (in the case of the chair conformer) or three water molecules (in the case of the linear conformer). The geometry and vibrational frequencies of PO_3^- without water were also computed using HF/6-31G(d). The resulting structures were then used as a starting point to compute the geometries and vibrational frequencies using HF/6-31G(d), B3LYP/6-31G(d) and B3LYP/6-31+G(d) levels of theory.

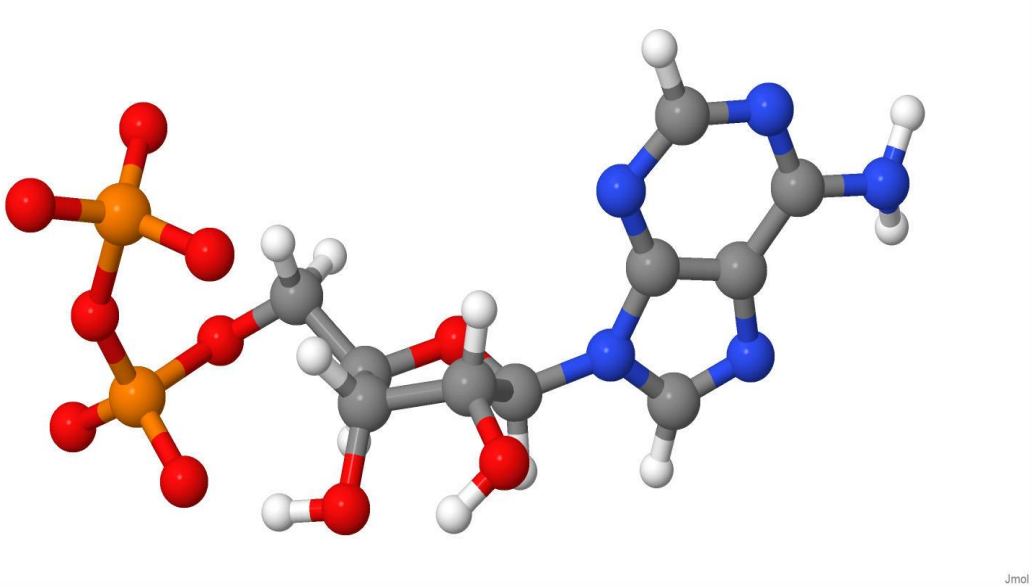

Figure 2.6 The optimized structure for the linear conformer of ADP^{3-} determined using the HF/6-31G(d) level of theory.

The phosphorylated glucose anion product geometry and vibrational frequencies were determined using HF/6-31G(d) with and without two water molecules included (to stabilize the two negative charges) by adding PO_3^- to the O^- site of the previously optimized $glucose^-$ conformer. The resulting structures (phosphorylated glucose anion in the gas phase is shown in Figure 2.7) were then used to calculate the geometries and vibrational frequencies using the HF/6-31+G(d), B3LYP/6-31G(d) and B3LYP/6-31+G(d) levels of theory.

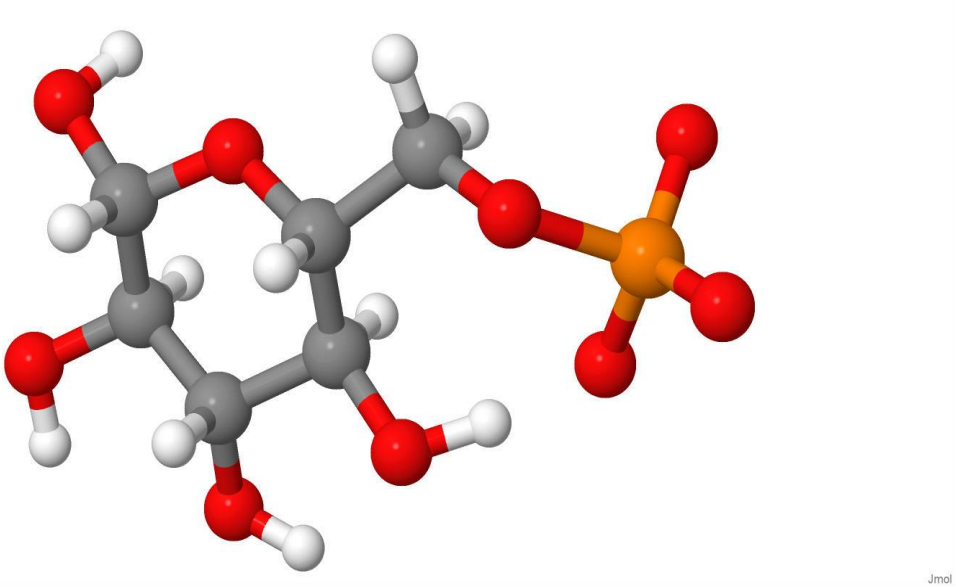

Figure 2.7 The optimized structure of the phosphorylated glucose anion in the gas phase using the HF/6-31G(d) level of theory.

The changes in enthalpy and entropy were determined using the thermochemistry output from the vibrational frequency calculations for each isomer of ATP^{4-} with and without the inclusion of water molecules. The change in Gibbs energy was calculated using Eq. 2.1.

$$\Delta G = \Delta H - T\Delta S \quad (2.1)$$

2.3 Transition States

Transition states for the first step involving the dissociation of ATP^{4-} into ADP^{3-} and PO_3^- were achieved by stretching the terminal P-O bond distance of ATP^{4-} out to about 2.9 Å, which is the optimal distance as previously reported. [20] Initially, this distance had to be frozen for the proper transition stated to be achieved. The bond distance was then allowed to be activated to get the fully optimized transition state. As the transition state for the chair conformer is also prone to a proton transfer, the O-H bond distance of the ribose sugar had to first be frozen to achieve the proper transition state. After the transition state was located, the O-H bond distance was then allowed to be relaxed giving the fully optimized transition state (an example is shown in Figure 2.8) for the chair conformer.

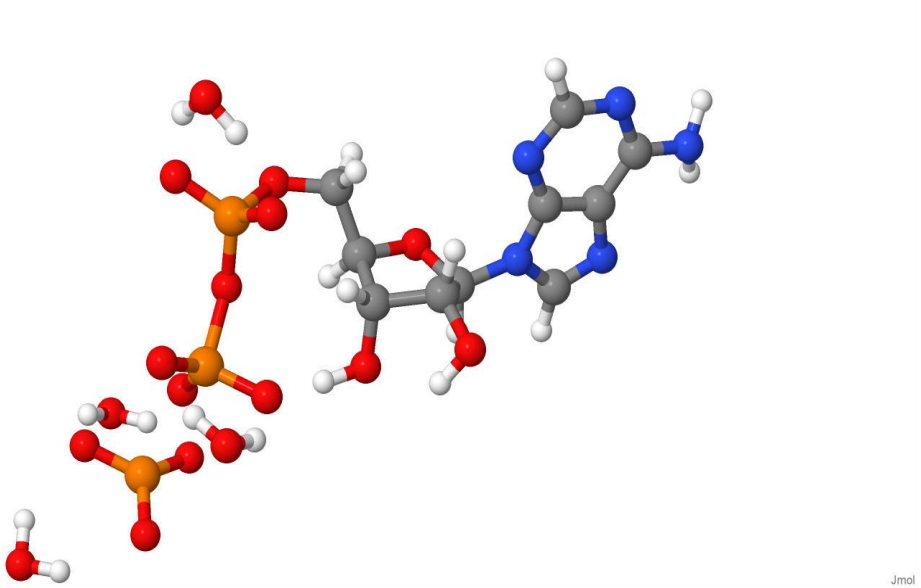

Figure 2.8 The optimized first step transition state structure for the chair conformer using the HF/6-31G(d) level of theory.

Transition states for the second step involving the formation of the phosphorylated glucose anion from the glucose anion and PO_3^- were achieved by increasing the P-O bond

distance of the phosphorylated glucose anion out to about 3.5 Å, which is the optimal distance as previously reported. [20] As with the transition states for the first step, this bond distance had to be initially frozen (an example is shown in Figure 2.9) and then the structure re-optimized with the bond distance relaxed to achieve the fully optimized transition states.

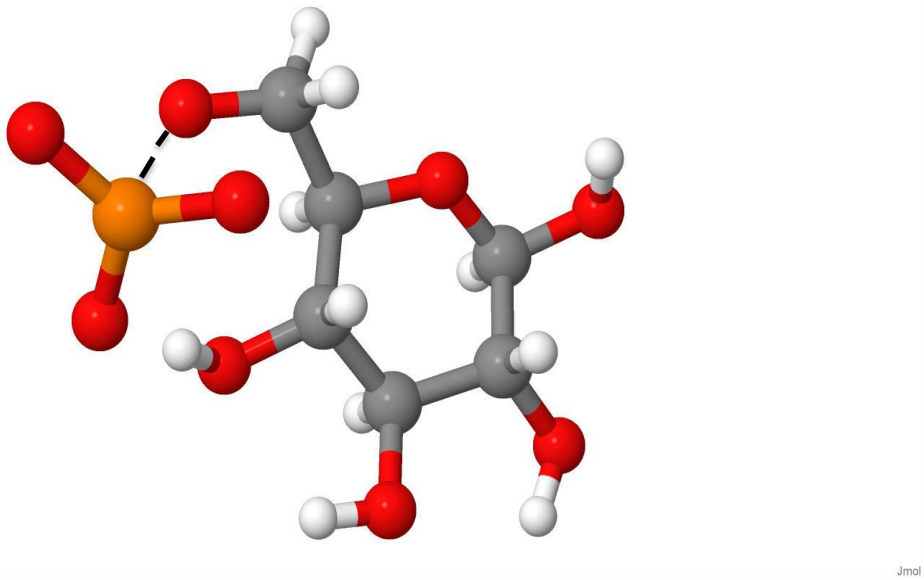

Figure 2.9 The resulting structure for the second step transition state using the HF/6-31G(d) level of theory keeping the O17-P18 bond length frozen. The O17-P18 bond is shown as a black dashed line.

3. Conformational Analysis and Dephosphorylation Mechanism of ATP^{4-}

3.1 Chair vs. Linear

The results for the potential energy surface (PES) scan of both the chair (sample structures are shown in Figure 3.1) and linear conformers of ATP^{4-} show that a local lowest energy structure for each conformer was indeed obtained by the *ab initio* calculations performed using Gaussian 09 (see Appendices I and II).

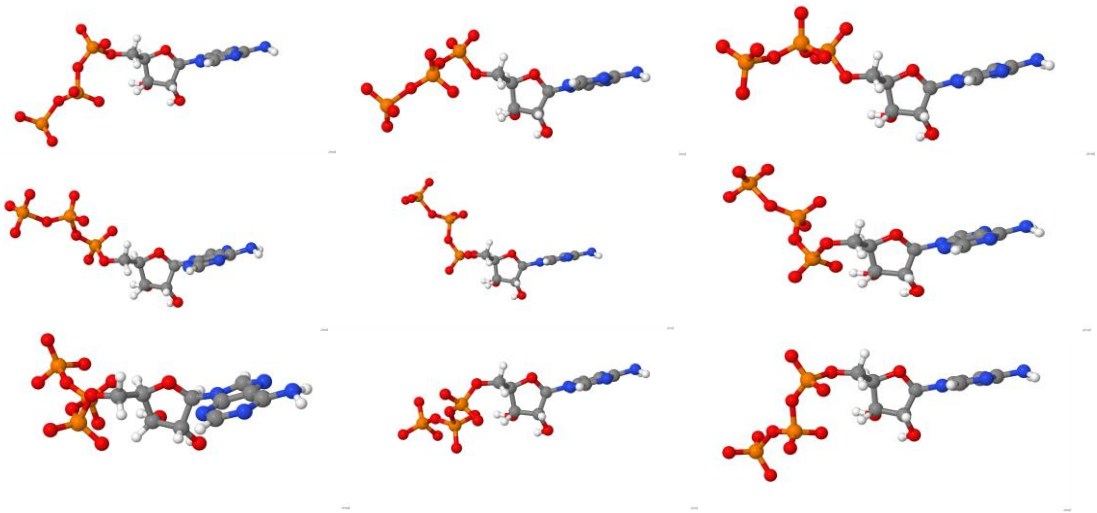

Figure 3.1 PES scan around the C-C-O-P torsional angle of the chair conformer of ATP^{4-} in increments of 40° from left to right, top to bottom.

As seen in previous conformational studies on ATP, [14-18] the chair conformer was found to be more stable than the linear conformer both with and without the inclusion of four water molecules (see Table 3.1 and Appendices III-VI). The addition of diffuse functions decreased the energy difference between the two conformers using both HF and B3LYP. With almost all levels of theory, the inclusion of four water molecules lowered the energy difference between the two conformers except when using the B3LYP/6-31+G(d) level of theory. All the energy differences between the two conformers are relatively similar using the various levels of theory, except for ATP^{4-} without water

molecules using the B3LYP/6-31G(d) level of theory, which can be attributed to the discovery of a new isomer of ATP^{4-} that occurred for the chair conformer, which is discussed in Section 3.2.

Table 3.1 Relative Energies (in kJ mol^{-1}) of the Linear Conformer of ATP^{4-} with Respect to the Chair Conformer of ATP^{4-}

	Level of Theory			
Conformer	HF/ 6-31G(d)	HF/ 6-31+G(d)	B3LYP/ 6-31G(d)	B3LYP/ 6-31+G(d)
Chair ATP^{4-}	0.0	0.0	0.0	0.0
Linear ATP^{4-}	+39.9	+32.0	+116.8 [a]	+8.4
Chair $ATP^{4-}\cdot 4H_2O$	0.0	0.0	0.0	0.0
Linear $ATP^{4-}\cdot 4H_2O$	+32.6	+28.4	+32.5	+25.9

[a] Chair ATP^{4-} changed into a new isomer during this calculation.

3.2 A New Isomer of ATP^{4-}

While doing the PES scan for the chair conformer of ATP^{4-}, it was discovered that the proton of one of the O-H groups on the ribose sugar was capable of transferring to the negatively charged oxygen atom on the middle phosphoryl group of the chain (shown in Figure 3.2). This proton transfer was also observed when performing the geometry optimizations for the chair conformer without diffuse functions and without water added using the B3LYP functional. However, this proton transfer was not observed while running the geometry optimizations for the chair conformer upon the inclusion of water molecules. It was then decided to run the energy calculations for this new "chairPT" isomer and compare it to the results obtained for the chair conformer of ATP^{4-}.

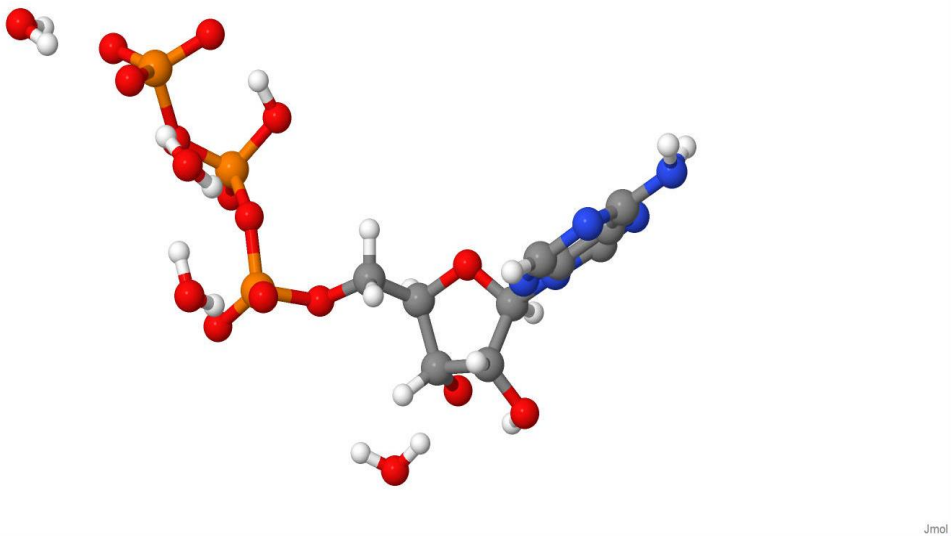

Figure 3.2 Structure obtained for the proton transfer isomer of ATP^{4-} run using HF/6-31G(d) with four water molecules included.

It was determined that proton transfer isomer of ATP^{4-} was consistently lower in energy than the chair conformer of ATP^{4-} both with and without the inclusion of four water molecules (see Table 3.2 and Appendices III-VI). The structure for the chairPT

ATP^{4-} isomer could not be optimized without water molecules included using the B3LYP functional, since the bond between the terminal phosphate group and the middle phosphate group breaks and the unattached phosphate group moves out to an infinite distance. The differences in energies between the two forms of ATP^{4-} is consistent upon the inclusion of four water molecules, although they are slightly lower using the B3LYP functional. Also, including diffuse functions for the proton transfer isomer of ATP^{4-} did not significantly change the energy differences between the two isomers and in most cases led to a slightly greater energy difference between the two isomers.

Table 3.2 Relative Energies (in kJ mol^{-1}) of the Proton Transfer Isomer of ATP^{4-} with Respect to the Chair Conformer of ATP^{4-}

	Level of Theory			
Isomer	HF/ 6-31G(d)	HF/ 6-31+G(d)	B3LYP/ 6-31G(d)	B3LYP/ 6-31+G(d)
Chair ATP^{4-}	0.0	0.0	0.0	0.0
ChairPT ATP^{4-}	-200.0	-190.8	- [a]	- [a]
Chair $ATP^{4-}\cdot 4H_2O$	0.0	0.0	0.0	0.0
ChairPT $ATP^{4-}\cdot 4H_2O$	-102.5	-107.3	-91.6	-102.3

[a] Unable to determine structures due to infinite separation of the terminal phosphate from ATP^{4-} during these calculations.

3.3 Dephosphorylation of ATP^{4-}

The mechanism for the dephosphorylation of both the chair and chairPT isomers of ATP^{4-} was examined. The reaction (eq. 3.1) was looked at both with and without the presence of water molecules in the gas phase.

$$ATP^{4-}_{(g)} \rightarrow ADP^{3-}_{(g)} + PO_3^{-}{}_{(g)} \quad (3.1)$$

3.3.1 Activation Energies

Without water molecules added, the transition states were unable to be obtained for the chair isomer of ATP^{4-} since the proton transfer occurred during the calculations for both structures for all levels of theory. For the chairPT isomer, the transition states were able to be obtained without water molecules added using HF, but not for B3LYP due to the separation of the terminal phosphate described in Section 3.2. The activation energy to go from the chairPT isomer of ATP^{4-} to the transition state for the dephosphorylation of the chairPT isomer of ATP^{4-} without the inclusion of water molecules is quite small (see Table 3.3).

Table 3.3 ATP^{4-} Dephosphorylation Activation Energies (in kJ mol^{-1})

	Level of Theory			
Isomer	HF/ 6-31G(d)	HF/ 6-31+G(d)	B3LYP/ 6-31G(d)	B3LYP/ 6-31+G(d)
Chair ATP^{4-}	- [a]	- [a]	- [a]	- [a]
ChairPT ATP^{4-}	2.7	6.7	- [b]	- [b]
Chair $ATP^{4-}\cdot 4H_2O$	118.7	120.3	- [a]	- [a]
ChairPT $ATP^{4-}\cdot 4H_2O$	183.3	191.5	160.7	

[a] Chair ADP^{3-} dephosphorylation transition state unable to be obtained due to the proton transfer that occurs.
[b] ChairPT ATP^{4-} reactant unable to be obtained due to infinite separation of the terminal phosphate.

Upon inclusion of four water molecules, the transition states for the chair isomer of ATP^{4-} could only be determined using HF (see Figure 3.3 for the IRC for chair $ATP^{4-}\cdot 4H_2O$ using the HF/6-31G(d) level of theory; the forward IRC calculation stops after one point since it deems this point to be the PES minimum, but really this occurs at an infinite separation of ADP^{3-} from PO_3^-), since upon using the B3LYP functional the proton transfer occurs. As can be seen in Table 3.3, the activation energy is lower to go from the chair isomer of ATP^{4-} to the transition state for the dephosphorylation of the chair isomer of ATP^{4-} than it is to go from the chairPT isomer to the transition state for the dephosphorylation of the chairPT isomer of ATP^{4-} (see Figure 3.4 for the IRC for chairPT $ATP^{4-}\cdot 4H_2O$ using the HF/6-31G(d) level of theory; the forward IRC calculation stops after one point since it deems this point to be the PES minimum, but really this occurs at an infinite separation of ADP^{3-} from PO_3^-). This can be attributed to the fact that the chairPT isomer of ATP^{4-} is much lower in energy compared to the chair isomer of

ATP^{4-}, whereas the transition states for the dephosphorylation of the two isomers are closer in energy to one another. This could be because the separation of PO_3^- from ADP^{3-} for the chairPT isomer leads to a similar structure for the transition state as that for chairPT ATP^{4-}; whereas the separation of PO_3^- from ADP^{3-} for the chair isomer gave transition state structure having a slightly different orientation of the phosphate chain that is higher in energy. The transition state for the chair isomer would need to be re-run with the phosphate chain closer in orientation to the chair isomer of ATP^{4-} to see if the activation energy is lowered. The inclusion of four water molecules significantly increased the activation energy for the chairPT isomer of ATP^{4-}. This can be attributed to the fact that the addition of four water molecules greatly increased the stability of the chairPT isomer of ATP^{4-}, whereas the inclusion of four water molecules did not significantly increase the stability of the dephosphorylation transition state. It is possible that, without the presence of water molecules, the negative charge on the terminal oxygens of ADP^{3-} in the transition state are still partially stabilized by the phosphorus atom of the departing phosphate group. Therefore, the inclusion of four water molecules only further stabilizes the dephosphorylation transition state by a small amount.

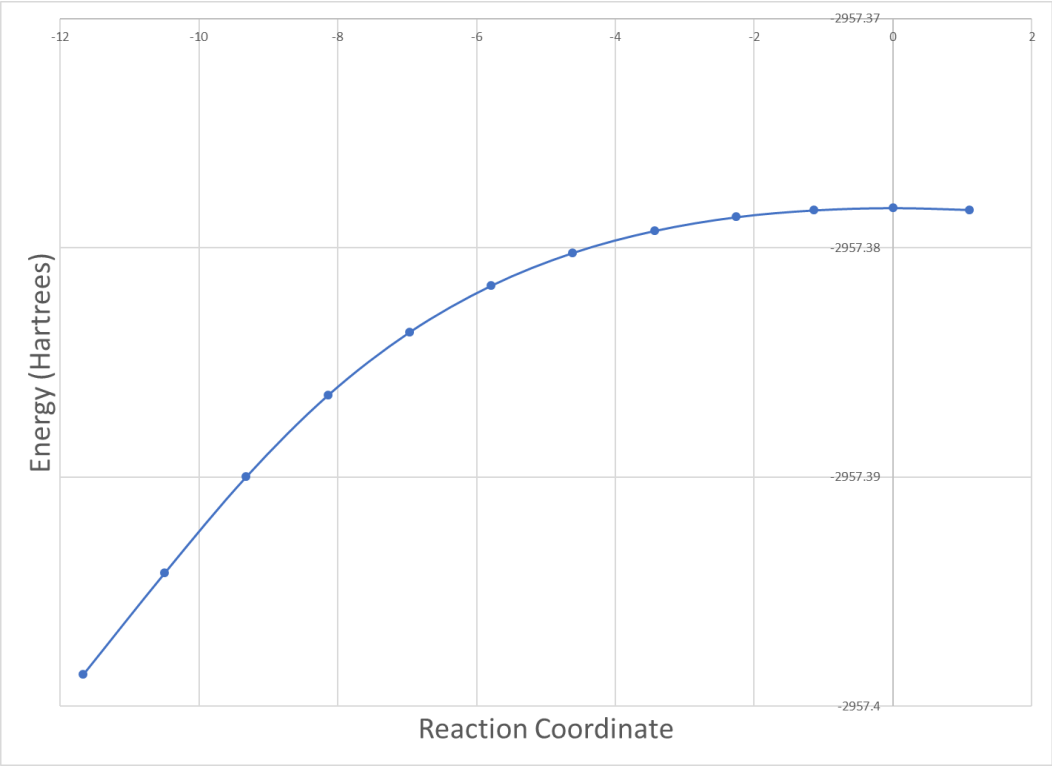

Figure 3.3 IRC for chair $ATP^{4-}\cdot 4H_2O$ using the HF/6-31G(d) level of theory.

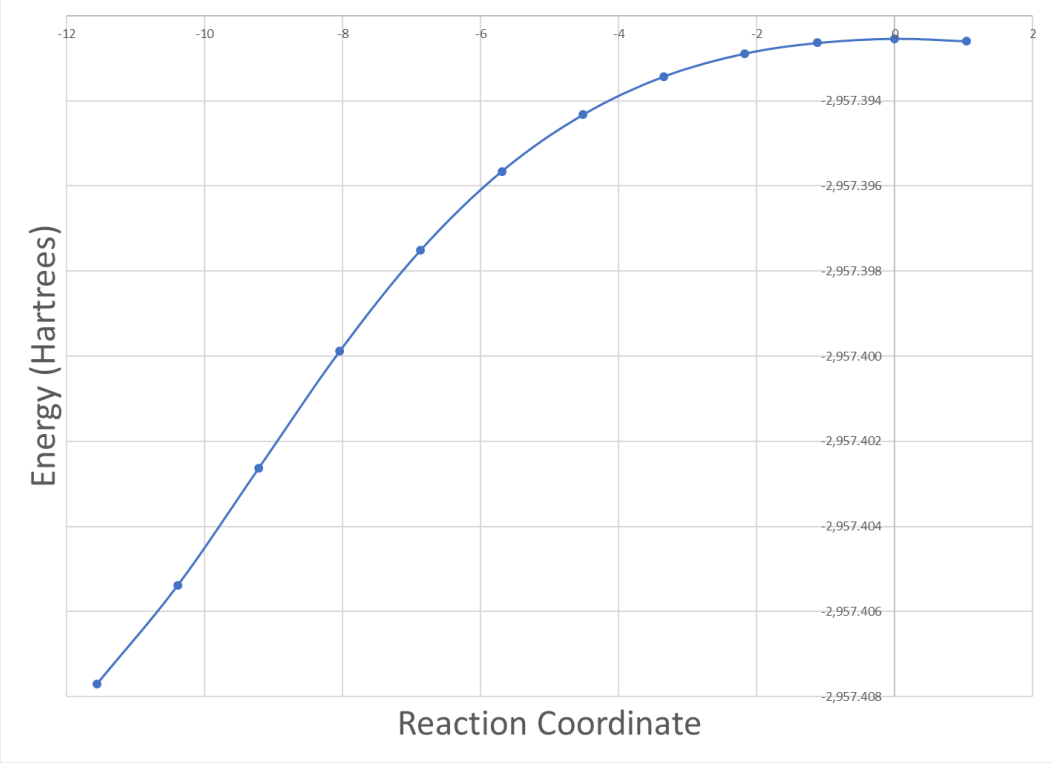

Figure 3.4 IRC for chairPT $ATP^{4-}\cdot 4H_2O$ using the HF/6-31G(d) level of theory.

The Gibbs energy of activation was also calculated for both the chair and chairPT conformers of ATP^{4-} with and without the inclusion of water using equation 2.1. Since the activation energy was quite small for the chairPT ATP^{4-} isomer without water included, it was expected that the Gibbs energy of activation would be small as well. As seen in Table 3.4, this was the result that was obtained.

Table 3.4 ATP^{4-} Dephosphorylation Gibbs Energies of Activation (in kJ mol^{-1})

	Level of Theory			
Isomer	HF/ 6-31G(d)	HF/ 6-31+G(d)	B3LYP/ 6-31G(d)	B3LYP/ 6-31+G(d)
Chair ATP^{4-}	- [a]	- [a]	- [a]	- [a]
ChairPT ATP^{4-}	1.5	4.2	- [b]	- [b]
Chair $ATP^{4-}\cdot 4H_2O$	87.3	88.0	- [a]	- [a]
ChairPT $ATP^{4-}\cdot 4H_2O$	167.6	171.0	147.0	

[a] Chair ADP^{3-} dephosphorylation transition state unable to be obtained due to the proton transfer that occurs.
[b] ChairPT ATP^{4-} reactant unable to be obtained due to infinite separation of the terminal phosphate.

Upon the inclusion of water molecules, the Gibbs energies of activation were larger for the chairPT isomer of ATP^{4-} than for the chair isomer of ATP^{4-} (as seen in Table 3.4). This result was expected, since the activation energies were smaller for the chair isomer of ATP^{4-} than for the chairPT isomer of ATP^{4-} (as seen in Table 3.3).

A fifth water molecule was added to the chair conformer of ATP^{4-} to see if it would significantly lower the activation energy. The resulting transition state using HF/6-31G(d) (see Figure 3.5a) only decreased the activation energy by about 3.2 kJ mol^{-1}. With the placement of the four water molecules in chair $ATP^{4-}\cdot 4H_2O$ (as shown in Figure 3.5b), all

the negative charge on the phosphate chain is stabilized by either a water molecule or from hydrogen bonding with the O-H of the sugar. This means that the addition of a fifth water molecule was not likely to significantly decrease the activation energy, which it did not.

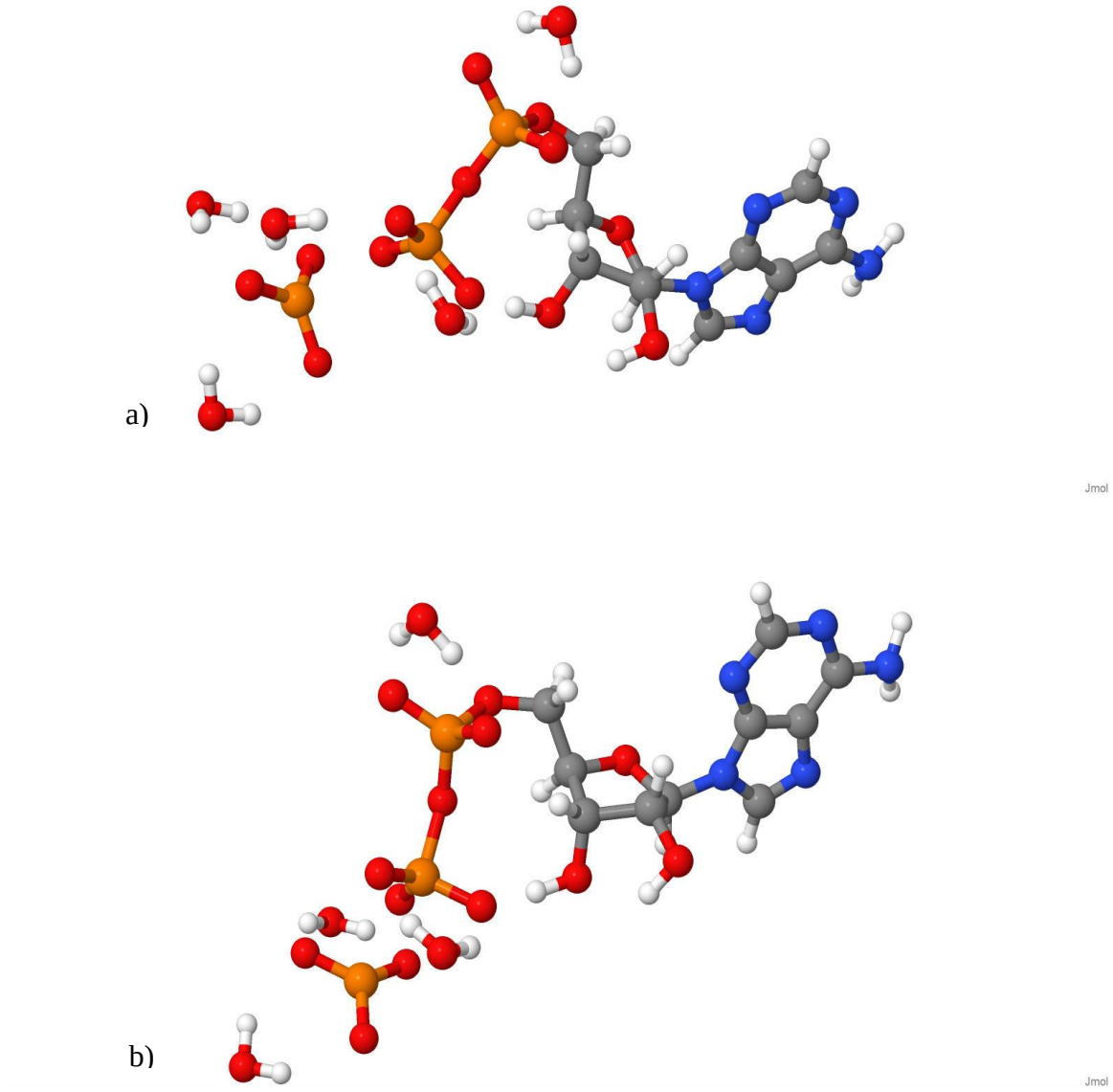

Figure 3.5 The transition states using the HF/6-31G(d) level of theory for a) chair $ATP^{4-}\cdot 4H_2O$ and b) chair $ATP^{4-}\cdot 5H_2O$.

3.3.2 Energy Changes

The change in energy (ΔU_{rxn}) values for the reaction of both isomers of ATP^{4-} dissociating into PO_3^- plus ADP^{3-} were determined both with and without the inclusion of four water molecules.

Without the inclusion of water molecules, the ADP^{3-} products for the chair isomer were unable to be obtained (see Table 3.5), since the proton transfer between the ribose sugar and the terminal phosphate group occurred using all levels of theory. For the chairPT isomer in the gas phase, all products were able to be obtained, although the energy change could not be determined using the B3LYP functional due to the terminal phosphate group separation described in Section 3.2. The inclusion of diffuse functions only slightly decreases the energy change for the reaction.

Table 3.5 ATP^{4-} Dephosphorylation Energy Changes (in kJ mol^{-1})

	Level of Theory			
Isomer	HF/ 6-31G(d)	HF/ 6-31+G(d)	B3LYP/ 6-31G(d)	B3LYP/ 6-31+G(d)
Chair ATP^{4-}	- [a]	- [a]	- [a]	- [a]
ChairPT ATP^{4-}	-557.2	-551.9	- [b]	- [b]
Chair $ATP^{4-}\cdot 4H_2O$	-396.1	-400.3	- [a]	- [a]
ChairPT $ATP^{4-}\cdot 4H_2O$	-460.3	-456.3	-468.2	-467.6

[a] Chair ADP^{3-} product unable to be obtained due to the proton transfer that occurs.
[b] ChairPT ATP^{4-} dephosphorylation energy unable to be calculated due to the infinite separation of the terminal phosphate for the chairPT ATP^{4-} reactant.

Upon the inclusion of four water molecules, the ΔU_{rxn} values for the dissociation of the chairPT isomer of ATP^{4-} is significantly less negative than without the presence of water

molecules using HF (as shown in Table 3.5). This could be due to the relative stability of the chairPT $ATP^{4-}\cdot 4H_2O$ reactant compared to the chairPT $ADP^{3-}\cdot 3H_2O$ and $PO_3^{-}\cdot H_2O$ products. Upon inclusion of four water molecules to chairPT ATP^{4-}, the energy of the reactant is significantly lowered (see Figures 3.6 and 3.7 for the reaction coordinate diagrams using the HF/6-31G(d) level of theory), which could be due to the ideal placement of the water molecules for hydrogen bonding. However, the inclusion of three water molecules for the chairPT isomer of ADP^{3-} does not lead to the same stabilization as the reactant, which could be due to a less favorable placement of the water molecules for hydrogen bonding. The ΔU_{rxn} for the dissociation of the chair ATP^{4-} isomer could not be determined using the B3LYP functional upon the inclusion of water molecules due to the proton transfer that occurs for the ADP^{3-} products. This could simply be due to the location of the water molecules. A change in positioning of the two water molecules might prevent this transfer from occurring and needs to be looked at.

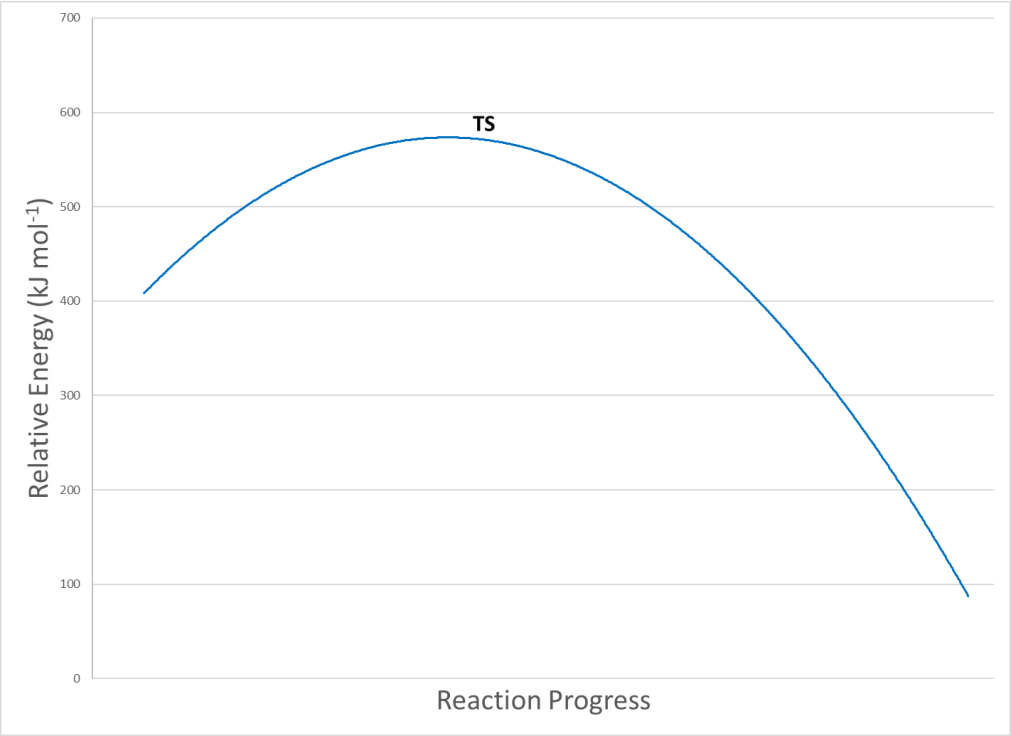

Figure 3.6 Reaction coordinate diagram for the dephosphorylation of chairPT ATP^{4-} using the HF/6-31G(d) level of theory.

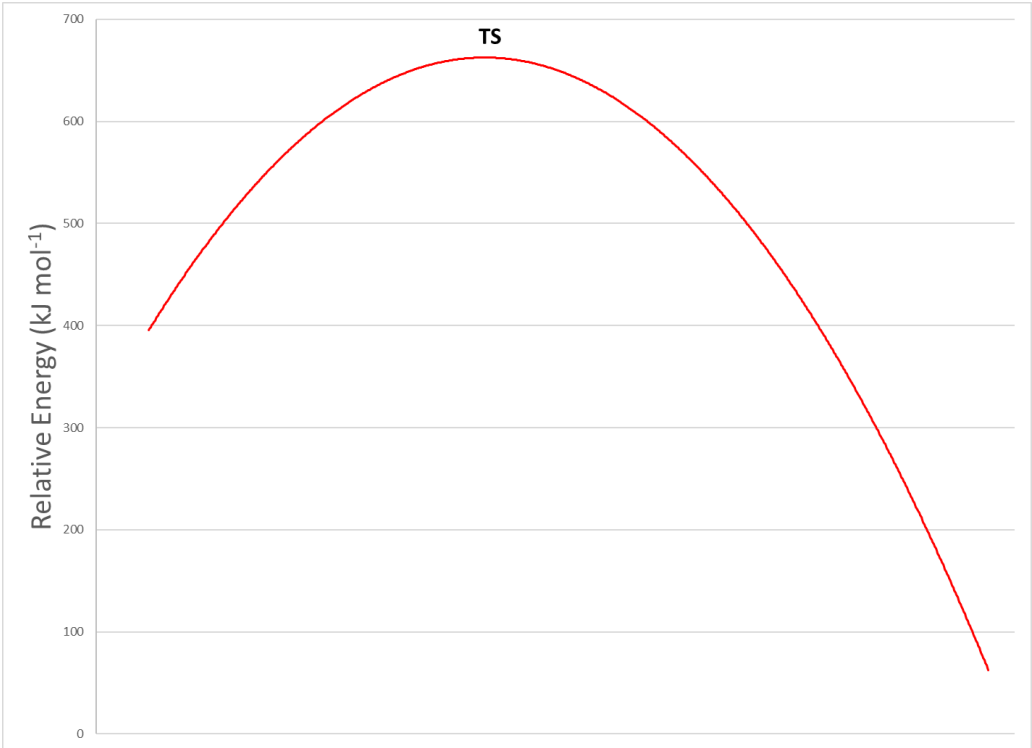

Figure 3.7 Reaction coordinate diagram for the dephosphorylation of chairPT $ATP^{4-}\cdot 4H_2O$ using the HF/6-31G(d) level of theory.

Comparing the energy changes for the dephosphorylation of chair $ATP^{4-}\cdot 4H_2O$ and chairPT $ATP^{4-}\cdot 4H_2O$, the energy changes for the chairPT isomer of $ATP^{4-}\cdot 4H_2O$ are greater than for the chair isomer of $ATP^{4-}\cdot 4H_2O$ using all levels of theory. The reaction coordinate diagram for both dephosphorylation reactions using the HF/6-31G(d) level of theory is shown in Figure 3.8. This could be because the chairPT isomer of $ATP^{4-}\cdot 4H_2O$ releases only one water molecule to hydrogen bond to the departing phosphate group, keeping three water molecules hydrogen bonded to the ADP^{3-} product, whereas the chair isomer of $ATP^{4-}\cdot 4H_2O$ releases two water molecules to hydrogen bond to the departing phosphate group, keeping only two water molecules hydrogen bonded to the ADP^{3-} product. This would seem to suggest that having more water molecules hydrogen bonded to the negative charges of the ADP^{3-} product is more stable than having more water molecules hydrogen bonded to the phosphate group. The inclusion of diffuse functions did not significantly affect the dephosphorylation energy changes.

Figure 3.8 Reaction coordinate diagram for the dephosphorylation of both the chair and chairPT isomers of $ATP^{4-}\cdot 4H_2O$ using the HF/6-31G(d) level of theory. Chair $ATP^{4-}\cdot 4H_2O$ is shown in blue and chairPT $ATP^{4-}\cdot 4H_2O$ is shown in red.

A fifth water molecule was added to the chair isomer of ATP^{4-} using the HF/6-31G(d) level of theory to see if there would be a significant difference in the ΔU_{rxn}. The addition of a fifth water molecule to the dephosphorylation reaction resulted in a slightly less negative ΔU_{rxn} than that with four water molecules (-396.1 kJ mol^{-1} for $ATP^{4-}\cdot 4H_2O$, -392.6 kJ mol^{-1} for $ATP^{4-}\cdot 5H_2O$). As with the transition state, the addition of a fifth water molecule did not result in any extra stabilization of the chair ADP^{3-} product.

The dephosphorylation reaction of ATP^{4-} is highly exothermic. This result makes sense, given that ATP is the energy currency of life. It can store lots of energy, which can

be released upon losing PO_3^-. This loss of energy can drive other reactions to occur or can change the shape of a protein and its ability to bind to another molecule. [34]

3.3.3 Changes in Enthalpy, Entropy and Gibbs Energy

The ΔH_{rxn}, ΔS_{rxn} and ΔG_{rxn} values could not be determined for the chair isomer of ATP^{4-} without the inclusion of water molecules since the ADP^{3-} products could not be determined due the proton transfer that occurs as seen previously in Section 3.3.2 for all levels of theory. Without water molecules included, the ΔH_{rxn}, ΔS_{rxn} and ΔG_{rxn} values could also not be determined for the chairPT isomer of ATP^{4-} using the B3LYP functional due to the separation of the terminal phosphate that occurs for chairPT ATP^{4-} as described in Section 3.2. The ΔH_{rxn}, ΔS_{rxn} and ΔG_{rxn} values could also not be determined with the inclusion of water molecules for the chair isomer of ATP^{4-} due to the proton transfer that occurs for the ADP^{3-} product as seen in Section 3.3.2. Tables 3.6, 3.7 and 3.8 show the ΔH_{rxn}'s, ΔS_{rxn}'s and ΔG_{rxn}'s respectively for the isomers of ATP^{4-} with and without the inclusion of water molecules.

Table 3.6 Changes in Enthalpy for the Dephosphorylation of ATP^{4-} (in kJ mol^{-1})

	Level of Theory			
Isomer	HF/ 6-31G(d)	HF/ 6-31+G(d)	B3LYP/ 6-31G(d)	B3LYP/ 6-31+G(d)
Chair ATP^{4-}	- [a]	- [a]	- [a]	- [a]
ChairPT ATP^{4-}	-556.3	-555.4	- [b]	- [b]
Chair $ATP^{4-}\cdot 4H_2O$	-406.0	-409.9	- [a]	- [a]
ChairPT $ATP^{4-}\cdot 4H_2O$	-465.9	-462.2	-473.0	-472.5

[a] Chair ADP^{3-} product unable to be obtained due to the proton transfer that occurs.
[b] ChairPT ATP^{4-} dephosphorylation energy unable to be calculated due to the infinite separation of the terminal phosphate for the chairPT ATP^{4-} reactant.

Table 3.7 Entropy Changes for the Dephosphorylation of ATP^{4-} (in J mol^{-1} K^{-1})

	Level of Theory			
Isomer	HF/ 6-31G(d)	HF/ 6-31+G(d)	B3LYP/ 6-31G(d)	B3LYP/ 6-31+G(d)
Chair ATP^{4-}	- [a]	- [a]	- [a]	- [a]
ChairPT ATP^{4-}	9.12	9.40	- [b]	- [b]
Chair $ATP^{4-}\cdot 4H_2O$	13.0	13.0	- [a]	- [a]
ChairPT $ATP^{4-}\cdot 4H_2O$	10.9	11.1	10.4	10.6

[a] Chair ADP^{3-} product unable to be obtained due to the proton transfer that occurs.
[b] ChairPT ATP^{4-} dephosphorylation energy unable to be calculated due to the infinite separation of the terminal phosphate for the chairPT ATP^{4-} reactant.

Table 3.8 ATP^{4-} Dephosphorylation Gibbs Energy Changes (in kJ mol^{-1})

	Level of Theory			
Isomer	HF/ 6-31G(d)	HF/ 6-31+G(d)	B3LYP/ 6-31G(d)	B3LYP/ 6-31+G(d)
Chair ATP^{4-}	- [a]	- [a]	- [a]	- [a]
ChairPT ATP^{4-}	-559.1	-558.3	- [b]	- [b]
Chair $ATP^{4-}\cdot 4H_2O$	-409.9	-413.7	- [a]	- [a]
ChairPT $ATP^{4-}\cdot 4H_2O$	-469.2	-465.5	-476.1	-475.6

[a] Chair ADP^{3-} product unable to be obtained due to the proton transfer that occurs.
[b] ChairPT ATP^{4-} dephosphorylation energy unable to be calculated due to the infinite separation of the terminal phosphate for the chairPT ATP^{4-} reactant.

As observed with the changes in energy in Section 3.3.2, the ΔH_{rxn} for the dephosphorylation of the chairPT isomer of ATP^{4-} was larger without the inclusion of water molecules than upon introducing water molecules. Upon the inclusion of water molecules, the ΔH_{rxn} for the dephosphorylation reaction is less negative for the chair isomer of ATP^{4-} than for the chairPT isomer of ATP^{4-}, like the result obtained for the ΔE_{rxn} in Section 3.2.2. For the chairPT isomer of ATP^{4-}, the ΔH_{rxn} is less negative upon the addition of water molecules than without water, like the result obtained for the ΔU_{rxn} in Section 3.2.2. The inclusion of diffuse functions makes the ΔH_{rxn} for the dephosphorylation of the chairPT isomer slightly less negative, while the inclusion of diffuse functions makes the ΔH_{rxn} for the dephosphorylation of the chair isomer slightly more negative.

The opposite trend is observed for the ΔS values. The ΔS_{rxn} is more positive for the dephosphorylation of the chairPT isomer of ATP^{4-} upon the introduction of water

molecules. The change in entropy can be computed using Eq. 3.2 and is based upon the change in quantity of heat (Δq) added to a system and the temperature (T) of a system. [33] The addition of water molecules to the system increases the number of energy levels available to particles in the system, meaning more heat is added to a system, which is turn causes a higher entropy at constant temperature. The ΔS_{rxn} for the dephosphorylation of the chair isomer of ATP^{4-} is more positive than for the dephosphorylation of the chairPT isomer of ATP^{4-}. The ΔS_{rxn} becomes more negative upon including diffuse functions for the dephosphorylation of the chairPT isomer of ATP^{4-}, while the introduction of diffuse functions produces the same ΔS_{rxn} for the dephosphorylation of the chair isomer of ATP^{4-} as without diffuse functions.

$$\Delta S = \Delta q / T \quad (3.2)$$

The above results show that the ΔG_{rxn} is more negative for the dephosphorylation of the chairPT isomer of ATP^{4-} without the presence of water molecules rather than with water. Upon the inclusion of water molecules, the ΔG_{rxn} is more negative for the dephosphorylation of the chairPT isomer of ATP^{4-} than for the dephosphorylation of the chair isomer of ATP^{4-}. The inclusion of diffuse functions results in a more negative ΔG_{rxn} for the dephosphorylation of the chair isomer of ATP^{4-}, while the change in ΔG_{rxn} for the dephosphorylation of the chairPT isomer of ATP^{4-} becomes less negative upon including diffuse functions. Using Eq. 2.1, a more negative ΔH and a more positive ΔS leads to a more negative ΔG, which is what is observed in Table 3.8.

As with the ΔU_{rxn} discussed in Section 3.3.2, the addition of a fifth water molecule led to a slightly less negative ΔH_{rxn}, a slightly less positive ΔS_{rxn} and a slightly less negative

ΔG_{rxn} (as seen in Table 3.9) for the dephosphorylation of the chair isomer of ATP^{4-} using the HF/6-31G(d) level of theory.

Table 3.9 Enthalpy, Entropy and Gibbs Energy Changes for the Dephosphorylation of Chair ATP^{4-} With Water Included Using the HF/6-31G(d) level of theory.

Compound	**ΔH (kJ mol^{-1})**	**ΔS (J mol^{-1} K^{-1})**	**ΔG (kJ mol^{-1})**
Chair $ATP^{4-}\cdot 4H_2O$	-406.0	13.0	-409.9
Chair $ATP^{4-}\cdot 5H_2O$	-400.5	12.6	-404.3

3.4 Feasibility of the ChairPT Isomer of ATP^{4-}

To determine the difficulty to get from one isomer to the other, the activation energy to get from the chair isomer of ATP^{4-} to the proton transfer isomer of ATP^{4-} was determined. This calculation was solely performed without the inclusion of water molecules (an example of the structure obtained is shown in Figure 3.9), since the proton transfer is not observed upon inclusion of water molecules. It was determined using HF (since the initial geometries for chair ATP^{4-} cannot be determined using B3LYP) that the activation energy for this process is quite small. Using the HF/6-31G(d) level of theory, the activation energy was calculated to be 1.4 kJ mol^{-1}.

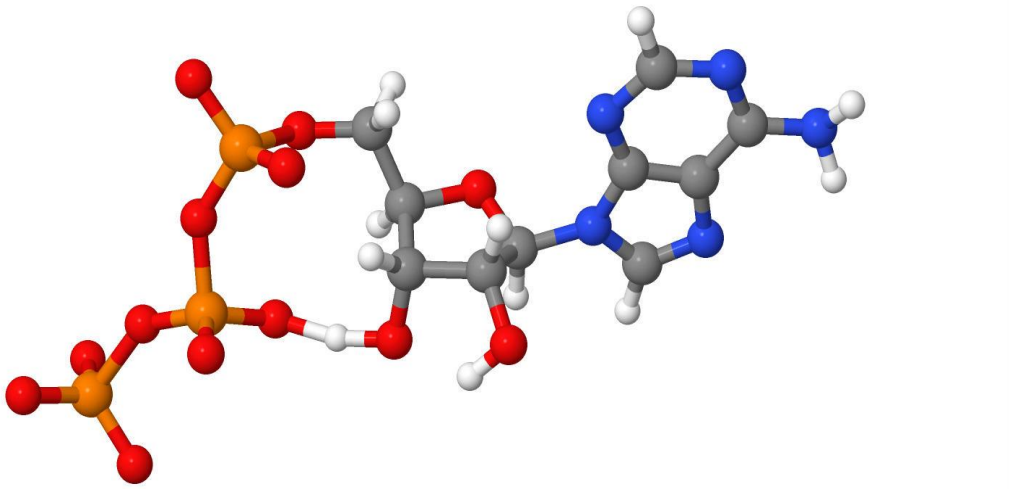

Figure 3.9 The transition state structure for the conversion of the chair isomer of ATP^{4-} to the proton transfer isomer of ATP^{4-} without the inclusion of water molecules calculated using the HF/6-31G(d) level of theory.

Since this energy barrier is so small and the energy gained by undergoing the proton transfer is so large, it is theoretically possible for this process to exist in nature. However, these calculations were done solely in the gas phase, these results bear little semblance to

the real world. Also, since this proton transfer does not occur during the calculations for ATP^{4-} with the inclusion of water molecules, which is a starting point to modelling the system in nature, and the activation energy is lower for the dephosphorylation of the chair isomer of ATP^{4-}, it is not likely that this process is seen in nature.

4. Conformational, Anomeric and Isomeric Analysis and Phosphorylation Mechanism of the Glucose Anion

4.1 Conformational Analysis of the Glucose Anion

Based upon previous studies, [23, 26] the deprotonated form of the GG conformer of the $^4C_1$ chair conformer of β-D-glucose was initially used as the starting reactant for the phosphorylation mechanism. Geometry optimizations and vibrational frequencies were calculated using HF and B3LYP. Calculations were done both with and without the inclusion of water molecules (glucose·$n$$H_2O$, where n is the number of water molecules).

However, previous studies done on the conformers of β-D-glucose were done for neutral glucose. The deprotonated form of glucose was chosen for this study since glucose is in the deprotonated form in the active site in the kanamycin studies done by Dr. Arpita Yadav's group due to a neighbouring aspartic acid residue. [20, 21] It was assumed that the GG conformer would still be the lowest energy conformer for the deprotonated form of β-D-glucose, but when the geometry optimization was completed, it was determined that the TG conformer of the β-D-glucose anion (see Figure 4.1 for the structure obtained using the HF/6-31G(d) level of theory) is lowest in energy. This can be explained by the presence of hydrogen bonding that occurs for the deprotonated form of the TG conformer of glucose. For the TG conformer of the β-D-glucose anion, hydrogen bonding can occur between the negatively charged oxygen of the deprotonated hydroxymethyl group and the nearest hydroxyl hydrogen on the ring. This lowers the energy for the TG conformer. Since this hydrogen bonding cannot occur for the other conformers of deprotonated β-D-glucose, the TG conformer of deprotonated β-D-glucose is the lowest energy conformer.

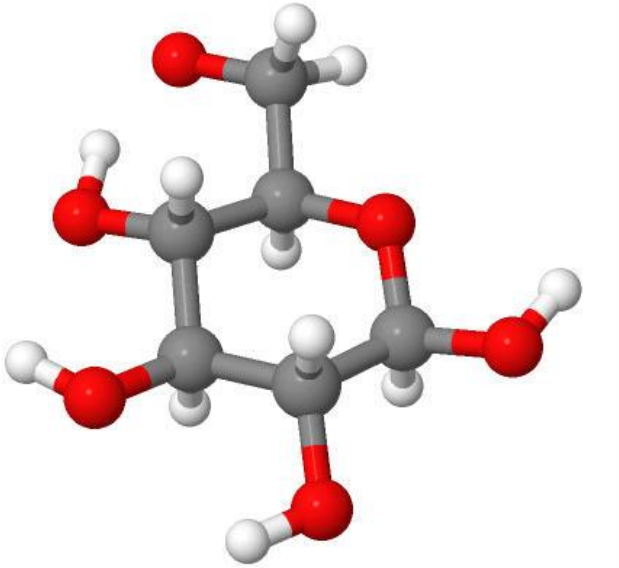

Figure 4.1 The structure obtained using the HF/6-31G(d) level of theory for the TG conformer of the β-D-glucose anion.

Therefore, the remainder of the calculations were performed using the TG conformer of glucose.

4.2 Anomeric and Isomeric Analysis of the Glucose Anion

Since a change in conformer was observed for the β-D-glucose anion, it was decided to ensure that β-D-glucose is the lowest energy anomer upon changing to the deprotonated form. Therefore, an anomeric analysis of both the α and β anomers and an isomeric analysis of both the D and L isomers of deprotonated glucose were performed to see the differences in the energies. Anomers are two sugars differing in configuration only at the carbonyl carbon in the open chain form, [36] whereas isomers are compounds that have the same molecular formula but different structures. [37]

The geometry optimizations and vibrational frequencies were calculated using both HF and B3LYP with and without diffuse functions. As can be seen in Table 4.1 and Appendices VII-X, the deprotonated form of β-D-glucose is lowest in energy both with and without water molecules using the HF/6-31+G(d) level of theory. Using the HF/6-31G(d) level of theory results in the deprotonated form of β-L-glucose being lowest in energy without including water molecules, while the deprotonated form of α-D-glucose is lowest in energy upon the inclusion of water molecules. Using the B3LYP functional results in the deprotonated form of β-L-glucose being lowest in energy in all cases.

Table 4.1 Energies of the Different Forms of the Glucose Anion Relative to the β-D-glucose Anion (in kJ mol^{-1})

Anion Anomer	**Level of Theory**			
	HF/ 6-31G(d)	HF/ 6-31+G(d)	B3LYP/ 6-31G(d)	B3LYP/ 6-31+G(d)
α-D-glucose	-0.27	3.32	-0.81	3.09
α-L-glucose	2.23	5.12	2.45	5.05
β-D-glucose	0.00	0.00	0.00	0.00
β-L-glucose	-0.41	0.16	-3.89	-2.71
α-D-glucose·H_2O	-0.96	2.75	-3.90	0.31
α-L-glucose·H_2O	1.04	4.11	-6.91	3.30
β-D-glucose·H_2O	0.00	0.00	0.00	0.00
β-L-glucose·H_2O	0.02	0.19	-34.62 [a]	-0.67

[a] Changed into a new isomer during calculation.

The energies of the various anomers and isomers of the glucose anion are within roughly 7 kJ mol^{-1} (as shown in Table 4.1 and Appendices VII-X) of each other. However, using the B3LYP/6-31G(d) level of theory with the inclusion of a water molecule, β-L-glucose$^-$·H_2O is far lower in energy than the other structures. This can be attributed to the discovery of a different isomer for the deprotonated form of glucose, which is discussed in Section 4.3.

4.3 A Different Isomer of the Glucose Anion

While running the calculations for the deprotonated form of the β-L-glucose·H_2O anion using the B3LYP/6-31G(d) level of theory (see Figure 4.2 for the resulting structure), it was determined that the proton on the hydroxyl group nearest to the CH_2O^- group was capable of transferring from the hydroxyl group to the negatively charged oxygen of the deprotonated hydroxymethyl group. This isomer is lower in energy, since having the negative charge on the ring allows for two sources of hydrogen bonding instead of one: one between the negatively charged oxygen and the hydrogen of the methoxy group and one between the negatively charged oxygen and the nearest hydroxyl group on the ring.

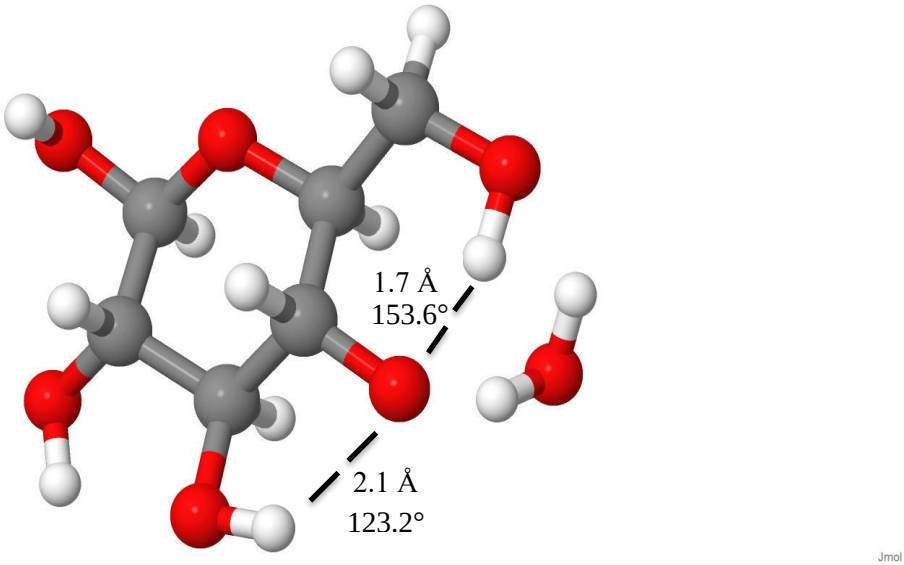

Figure 4.2 The different isomer obtained from the geometry optimization of the β-L-glucose·H_2O anion using the B3LYP/6-31G(d) level of theory. Hydrogen bonding is shown with the black dashed lines.

4.4 Phosphorylation of the Glucose Anion

Considering the generally small differences in energies between the various forms of deprotonated glucose with and without the inclusion of water, as well as the variation between the form of deprotonated glucose that is lowest in energy upon changing levels of theory and by including water molecules, it was decided that both the alpha and beta anomers and both the D and L isomers of deprotonated glucose would be chosen to study the phosphorylation reaction (Eq. 4.1) with and without the inclusion of water molecules.

$$C_6H_{11}O_6^-{}_{(g)} + PO_3^-{}_{(g)} \rightarrow C_6H_{11}PO_9^{2-}{}_{(g)} \quad (4.1)$$

4.4.1 Energy Changes

As can be seen in Table 4.2, without the presence of water molecules, the β-D-glucose anion has the least positive change in energy (ΔU_{rxn}) for the phosphorylation mechanism using all levels of theory. However, upon the inclusion of water molecules, the ΔU_{rxn} is lowest for the α-L-glucose·H_2O anion. This result is favourable for the prevention of phosphorylation from occurring inside the body. If the ΔU_{rxn} had to be the least positive for the β-D-glucose anion upon the inclusion of water molecules, which is the form of glucose most abundant in nature, [21] then phosphorylation would be more likely to occur inside the body. But, since nature is trying to prevent the phosphorylation of glucose from occurring, this result makes sense. The addition of diffuse functions to heavy atoms resulted in a slightly more positive ΔU_{rxn} for the phosphorylation reaction. Using HF resulted in slightly less positive ΔU_{rxn} values compared to the results obtained using the B3LYP functional. Using the B3LYP functional resulted in all the phosphorylated products undergoing the proton transfer described in Section 4.3, which is indicated by

the PT shown in Table 4.2. For the calculations of the phosphorylated products obtained using the B3LYP/6-31G(d) level of theory with water included, only the β-L-glucose·H_2O anion phosphorylated product underwent a proton transfer. The structure may simply require a change in the position of the water molecule and will be explored as part of future work. Therefore, the energy change for this form of phosphorylated glucose cannot be compared to the other forms of phosphorylated glucose and is omitted from Table 4.2.

Table 4.2 Changes in Energy for the Phosphorylation Mechanism of the Various Forms of the Deprotonated Glucose Anion (in kJ mol^{-1})

Anion Form	**Level of Theory**			
	HF/ 6-31G(d)	HF/ 6-31+G(d)	B3LYP/ 6-31G(d)	B3LYP/ 6-31+G(d)
α-D-glucose	119.1	127.7	131.1 (PT)	152.7 (PT)
α-L-glucose	118.0	128.8	134.8 (PT)	154.9 (PT)
β-D-glucose	113.6	123.0	129.4 (PT)	145.0 (PT)
β-L-glucose	118.0	127.6	140.8 (PT)	158.0 (PT)
α-D-glucose·H_2O	54.4	66.5	70.9	94.0
α-L-glucose·H_2O	36.4	58.5	38.1	73.0
β-D-glucose·H_2O	48.5	61.8	62.3	87.7
β-L-glucose·H_2O	52.1	67.9	- [a]	95.0

[a] Structure underwent a proton transfer during the calculation.

The relative ease of phosphorylation of the α-L-glucose·H_2O anion can be explained by the presence of hydrogen bonding that can solely exist for the L isomer of the phosphorylated glucose anion between the oxygen of one of the water molecules and the nearest hydroxyl hydrogen on the ring (as shown in Figure 4.3). The distance between the oxygen on the water molecule and the nearest hydroxyl hydrogen on the ring for the D

isomer of the phosphorylated glucose anion is too long for hydrogen bonding to occur. This hydrogen bonding results in a lower energy structure for the L isomer, but only upon the inclusion of water molecules. Since the energy for the β-L-glucose·H_2O anion is lower than the energy for the α-L-glucose·H_2O anion, the ΔU_{rxn} for the phosphorylation reaction is lowest for the α-L-glucose·H_2O anion.

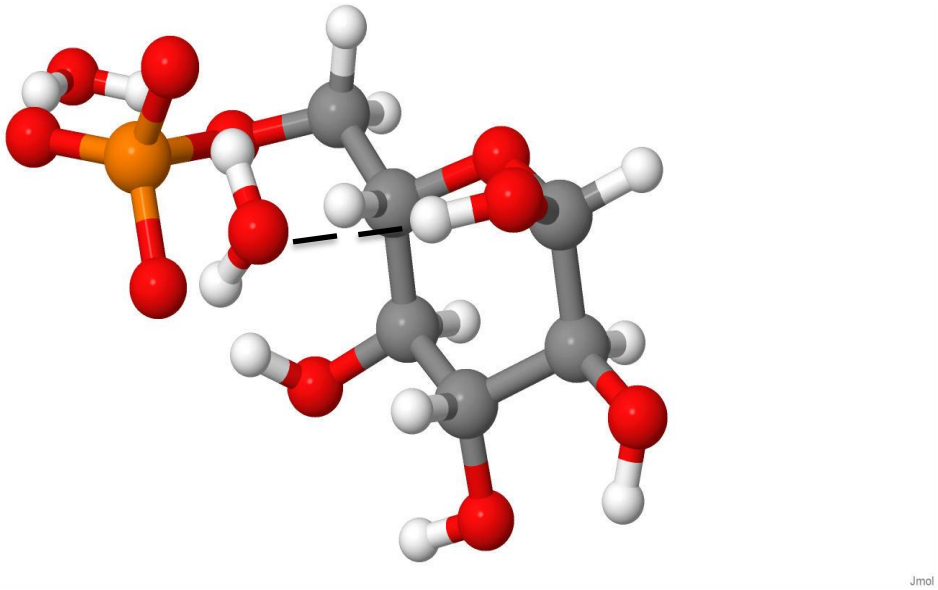

Figure 4.3 The structure obtained for phosphorylated α-L-glucose·$2H_2O$ anion using the HF/6-31G(d) level of theory. The additional hydrogen bond gained for the L isomer of phosphorylated glucose anion.

4.4.2 Changes in Enthalpy, Entropy and Gibbs Energy

As can be seen in Table 4.3, the β-D-glucose anion has the lowest ΔH_{rxn} without the inclusion of water molecules using all levels of theory. However, upon the inclusion of water molecules, the ΔH_{rxn} for the phosphorylation mechanism is generally less positive for the α-L-glucose·H_2O anion, except for the HF/6-31+G(d) level of theory where the change in enthalpy is roughly the same for both the α-L-glucose·H_2O anion and the β-D-glucose·H_2O anion. As with the ΔU_{rxn} discussed in Section 4.4.1, this result is favourable

for the prevention of phosphorylation from occurring inside the body. The changes in enthalpy were significantly lower upon the inclusion of water molecules. As with the ΔU_{rxn} values discussed in Section 4.4.1, the addition of diffuse functions made the ΔH_{rxn} values slightly more positive for the phosphorylation of deprotonated glucose. Using HF resulted in slightly less negative ΔH_{rxn} values than using the B3LYP functional.

Table 4.3 Changes in Enthalpy for the Phosphorylation of the Various Forms of the Deprotonated Glucose Anion (in kJ mol^{-1})

Anion Form	**Level of Theory**			
	HF/ 6-31G(d)	HF/ 6-31+G(d)	B3LYP/ 6-31G(d)	B3LYP/ 6-31+G(d)
α-D-glucose	126.3	135.3	135.6 (PT)	155.9 (PT)
α-L-glucose	127.0	137.4	138.6 (PT)	158.8 (PT)
β-D-glucose	120.8	130.7	133.1 (PT)	149.4 (PT)
β-L-glucose	127.2	136.7	144.4 (PT)	161.6 (PT)
α-D-glucose·H_2O	64.9	76.3	80.0	101.5
α-L-glucose·H_2O	49.7	71.9	51.4	85.8
β-D-glucose·H_2O	59.4	71.7	72.8	95.7
β-L-glucose·H_2O	63.3	88.8	- [a]	105.1

[a] Structure underwent a proton transfer during the calculation.

Without the inclusion of water molecules, the ΔS_{rxn} values (as seen in Table 4.4) are consistent for all forms of deprotonated glucose using all levels of theory with no significant differences. Some slight differences are that the ΔS_{rxn} values for the phosphorylation of the β-L-glucose anion are slightly more negative than the other forms using HF and the ΔS_{rxn} for the phosphorylation of the α-D-glucose anion is slightly less negative than the other forms using the B3LYP/6-31+G(d). In the presence of water

molecules, the ΔS_{rxn} values using all levels of theory are more negative for the α-L-glucose·H_2O anion. Unlike the ΔH_{rxn} values for the phosphorylation of deprotonated glucose, this is not encouraging since a more negative ΔS_{rxn} means that the α-L-glucose anion would not be more susceptible to phosphorylation in the body than the β-D-glucose anion as it would lead to a more positive value for the ΔG_{rxn} according to Eq. 2.1. The inclusion of water molecules resulted in slightly more negative ΔS_{rxn} values. The addition of diffuse functions did not greatly affect the ΔS_{rxn} values using HF. However, upon their inclusion using the B3LYP functional, it led to slightly less negative ΔS_{rxn} values for the phosphorylation of the α-D-glucose anion and in the presence of water molecules for the β-D-glucose anion, whereas it led to a slightly more negative ΔS_{rxn} for the phosphorylation of the α-L-glucose anion in the presence of water. The ΔS_{rxn} values were consistent regardless of whether HF or B3LYP was used.

Table 4.4 Changes in Entropy for the Phosphorylation of the Various Forms of the Deprotonated Glucose Anion (in J mol^{-1} K^{-1})

Anion Form	**Level of Theory**			
	HF/ 6-31G(d)	HF/ 6-31+G(d)	B3LYP/ 6-31G(d)	B3LYP/ 6-31+G(d)
α-D-glucose	-10.8	-10.7	-10.7 (PT)	-9.82 (PT)
α-L-glucose	-10.8	-10.8	-10.4 (PT)	-10.3 (PT)
β-D-glucose	-10.9	-10.7	-10.1 (PT)	-10.4 (PT)
β-L-glucose	-11.1	-11.1	-10.4 (PT)	-10.4 (PT)
α-D-glucose·H_2O	-12.4	-12.5	-12.6	-11.8
α-L-glucose·H_2O	-13.6	-14.1	-13.3	-14.4
β-D-glucose·H_2O	-12.5	-12.5	-12.7	-11.9
β-L-glucose·H_2O	-12.1	-12.6	- [a]	-12.8

[a] Structure underwent a proton transfer during the calculation.

Using the results for the ΔH_{rxn} and ΔS_{rxn} values and Eq. 2.1, the ΔG_{rxn} values are least positive for the phosphorylation of the β-D-glucose anion without the presence of water and that the ΔG_{rxn} values are generally less positive for the phosphorylation of the α-L-glucose anion upon the inclusion of water molecules, as is shown in Table 4.5. These results suggest that the ΔH_{rxn} has a larger effect on the ΔG_{rxn} than the ΔS_{rxn} for the phosphorylation of deprotonated glucose. Therefore, the ΔG_{rxn} values are favourable for the prevention of the phosphorylation of glucose inside the body, since upon the inclusion of water molecules, the ΔG_{rxn} values are less positive for the α-L-glucose anion and not the β-D-glucose anion. The inclusion of diffuse functions led to less positive ΔG_{rxn} values using both HF and B3LYP. The inclusion of water molecules made the ΔG_{rxn} values for the phosphorylation of deprotonated glucose significantly less positive due to the less

positive ΔH_{rxn} values upon including water. The ΔG_{rxn} values were more positive using the B3LYP functional than for HF, which is due to the more positive ΔH_{rxn} values using B3LYP. Since the ΔG_{rxn} values are all positive indicating a non-spontaneous phosphorylation reaction, the driving factor comes from the dephosphorylation of ATP^{4-}. (32)

Table 4.5 Changes in Gibbs Energy for the Phosphorylation of the Various Forms of the Deprotonated Glucose Anion (in kJ mol^{-1})

Anion Form	**Level of Theory**			
	HF/ 6-31G(d)	HF/ 6-31+G(d)	B3LYP/ 6-31G(d)	B3LYP/ 6-31+G(d)
α-D-glucose	129.5	138.5	138.8 (PT)	158.8 (PT)
α-L-glucose	130.2	140.6	141.7 (PT)	161.9 (PT)
β-D-glucose	124.0	133.9	136.2 (PT)	152.5 (PT)
β-L-glucose	130.5	140.0	147.5 (PT)	164.7 (PT)
α-D-glucose·H_2O	68.6	80.0	83.8	105.0
α-L-glucose·H_2O	53.8	76.1	55.4	90.0
β-D-glucose·H_2O	63.1	75.5	76.6	99.3
β-L-glucose·H_2O	66.9	92.6	- [a]	109.0

[a] Structure underwent a proton transfer during the calculation.

4.5 Feasibility of Anomer and Isomer Conversions

4.5.1 Feasibility of the α-L-glucose Anion in the Phosphorylation Mechanism

As has been previously reported, [23] β-D-glucose is the form of glucose found in the body. If this is indeed true for the deprotonated form of glucose, then for the α-L-glucose anion to be the form of glucose involved in the phosphorylation mechanism, two conversions would need to be performed: the conversion of deprotonated beta glucose to deprotonated alpha glucose and the conversion of deprotonated D glucose to deprotonated L glucose.

The conversion from deprotonated β-glucose to deprotonated α-glucose can be explained relatively easily. Glucose can exist in equilibrium between three structures: the alpha anomer, the open chain form and the beta anomer. Starting from the open chain form, if the OH group at the anomeric carbon is pointing down, then α-D-glucose will be formed. Starting from the open chain form, if the OH at the anomeric carbon is pointing up, then β-D-glucose will be formed. The same principles apply for the deprotonated form of these species. In the presence of water, which can act as a weak base, the β-D-glucose anion can be converted to the open chain form upon removing a proton from the OH group of the anomeric carbon. Then the conversion to the α-D-glucose anion can happen by reforming the ring and then protonation of the C=O bond from above by the newly formed H_3O^+ acid. However, this conversion cannot occur without the initial presence of a base, such as water, so this anomer switch would only occur upon inclusion of water molecules or other bases. [36]

There have been several studies done involving the conversion of D-glucose to L-glucose. Sowa synthesized L-glucurone from D-*glycero*-D-*gulo*-heptonolactone (as shown

in Scheme 4.1). Since L-glucose can be prepared from L-glucurone and D-*glycero*-D-*gulo*-heptonolactone can be made starting with D-glucose, D-glucose can be transformed into L-glucose. [38]

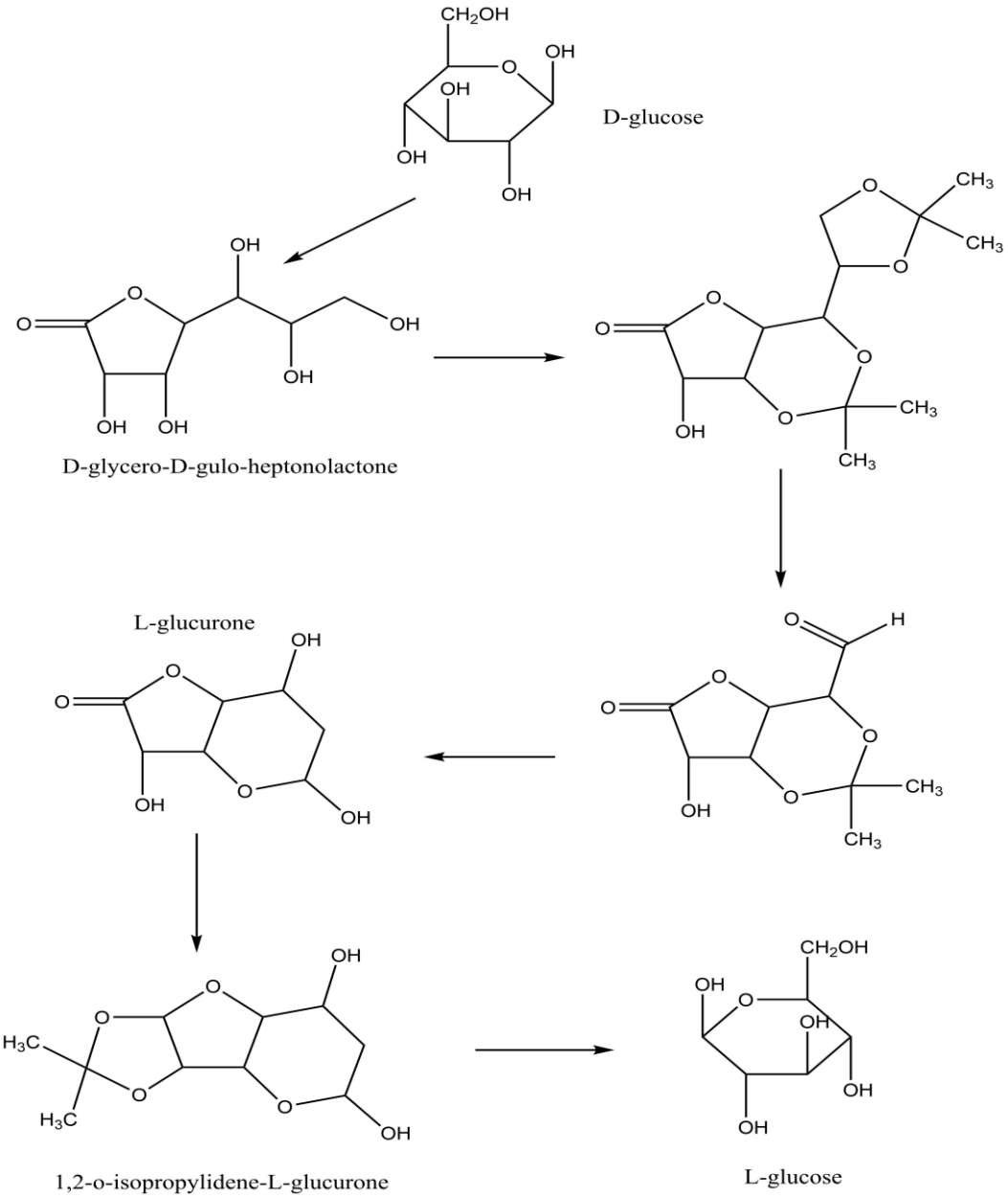

Scheme 4.1 Conversion of D-glucose to L-glucose through L-glucurone.

Shiozaki used 2,3,4,6-tetra-O-benzyl-D-glucono-1,5-lactone as a starting material to synthesize 2,3,4-tri-O-benzyl-1-O-(3-chlorobenozyl)-6-O-(trimethylacetyl)-β-L-glucopyranose using oxidative decarboxylation (as shown in Scheme 4.2). Since D-glucose was used to prepare 2,3,4,6-tetra-O-benzyl-D-glucono-1,5-lactone and L-glucose can be derived from 2,3,4-tri-O-benzyl-1-O-(3-chlorobenozyl)-6-O-(trimethylacetyl)-β-L-glucopyranose, D-glucose can be converted into L-glucose. [39]

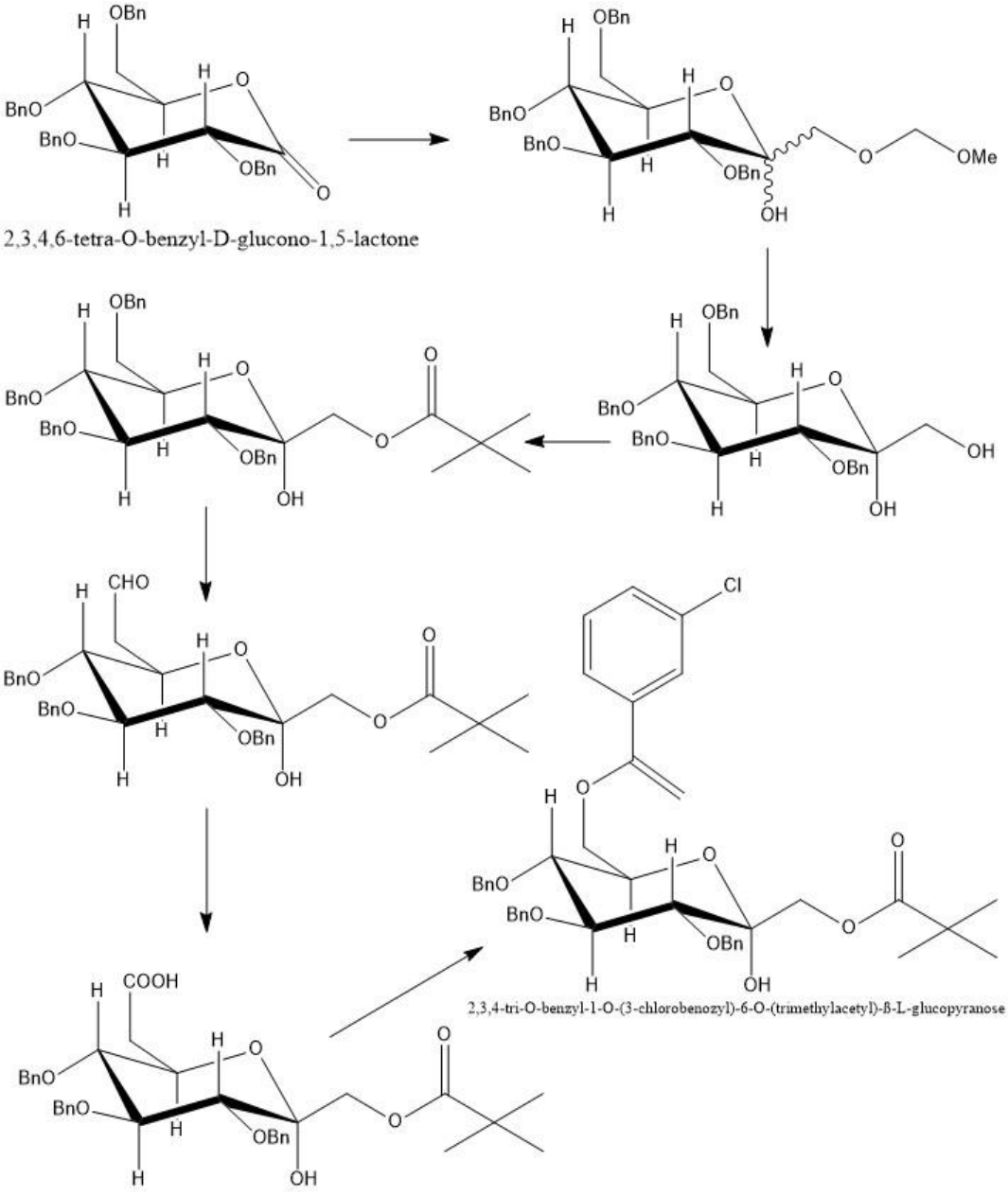

Scheme 4.2 Synthesis of 2,3,4-tri-O-benzyl-1-O-(3-chlorobenozyl)-6-O-(trimethylacetyl)-β-L-glucopyranose from 2,3,4,6-tetra-O-benzyl-D-glucono-1,5-lactone. (Adapted with permission from reference 39. Copyright 2018 American Chemical Society)

Even though D-glucose can be converted into L-glucose in a laboratory, it remains to be seen how this transformation could occur in the body. It is possible that there could be the presence of an enzyme that would facilitate this process. It is possible that there is a

different reaction pathway that is more feasible that occurs in nature. It is also equally or more possible that this conversion does not occur at all and that deprotonated β-D-glucose is always present within the body. If this is the situation, then the phosphorylation of glucose is not as likely to occur due to the less positive ΔU_{rxn}, ΔH_{rxn} and ΔG_{rxn} values for the phosphorylation of the β-D-glucose anion than for the phosphorylation of the α-L-glucose anion, thus supporting the initial purpose of this project in determining how to prevent drug modification (in this case phosphorylation) of antibiotics. The structure for the transition state of the conversion from D-glucose to L-glucose as well as its activation energy would need to be determined to clearly answer the question about the feasibility of the conversion from the β-D-glucose anion to α-L-glucose anion.

4.5.2 Feasibility of the Proton Transfer Isomer of the Glucose Anion

To determine the difficulty in going from the normal isomer to the proton transfer isomer of deprotonated glucose, the transition states (see Figure 4.4 for the structure of the proton transfer isomer of the β-D-glucose anion using the HF/6-31G(d) level of theory) and activation energies were determined for each form of the proton transfer isomer of deprotonated glucose. As shown in Table 4.3, the activation energy to go from the normal isomer to the proton transfer isomer of the glucose anion is quite small for all forms of glucose using the HF/6-31G(d) level of theory, as was observed for the conversion of the chair isomer of ATP^{4-} to the chairPT isomer of ATP^{4-} seen in Section 3.4.

Table 4.6 Activation Energies (in kJ mol^{-1}) using the HF/6-31G(d) Level of Theory for the Conversion of the Glucose Anion to the Proton Transfer Isomer of the Glucose Anion

Anion Form	Activation Energy
α-D-glucose	6.9
α-L-glucose	6.8
β-D-glucose	6.3
β-L-glucose	5.5

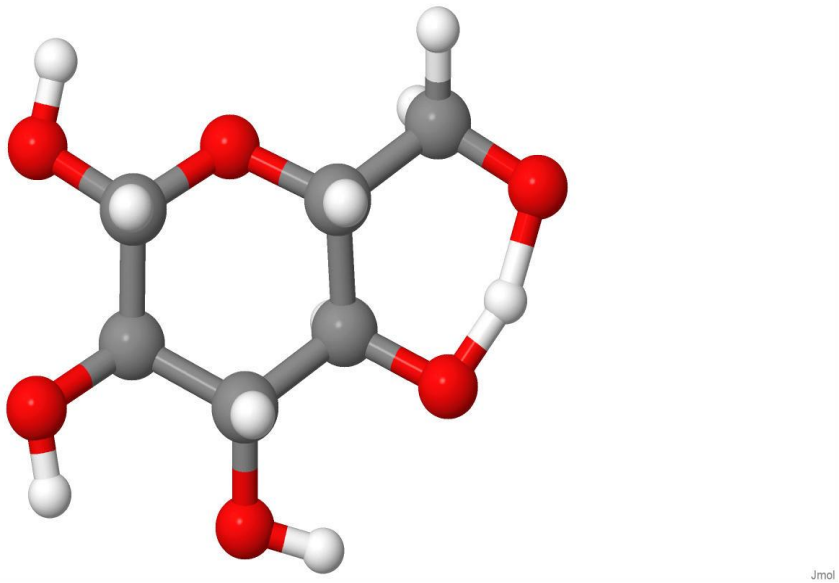

Figure 4.4 The transition state structure for the conversion of the β-D-glucose anion to the proton transfer isomer of β-D-glucose anion using the HF/6-31G(d) level of theory.

However, the proton transfer is only observed during geometry optimization calculations using the B3LYP functional. Also, this proton transfer was generally only observed during the calculations without the inclusion of water molecules. Therefore, as is the case with the proton transfer isomer of ATP^{4-} discussed in Section 3.4, it is not likely that isomerization occurs in the body.

5. Conclusions

The chair conformer of ATP^{4-} was found to be lower in energy than the linear conformer of ATP^{4-}. A new chairPT isomer of ATP^{4-} was found to be lower in energy than the chair isomer of ATP^{4-}. The activation energy for the dephosphorylation of chairPT isomer of ATP^{4-} was determined to be lower for chairPT ATP^{4-} than for chairPT $ATP^{4-}\cdot 4H_2O$. The activation energy for the dephosphorylation of ATP^{4-} was found to be lower for chair $ATP^{4-}\cdot 4H_2O$ than for chairPT $ATP^{4-}\cdot 4H_2O$. For the dephosphorylation of the chairPT isomer ATP^{4-}, it was determined that the ΔU_{rxn}, ΔH_{rxn} and ΔG_{rxn} were more negative for chairPT ATP^{4-} than for chairPT $ATP^{4-}\cdot 4H_2O$. The ΔU_{rxn}, ΔH_{rxn} and ΔG_{rxn} for the dephosphorylation of ATP^{4-} were found to be more negative for the chairPT $ATP^{4-}\cdot 4H_2O$ than for the chair $ATP^{4-}\cdot 4H_2O$. The addition of a fifth water molecule to the chair isomer of ATP^{4-} did not significantly affect the activation energy, ΔU_{rxn}, ΔH_{rxn}, ΔS_{rxn} or ΔG_{rxn} for the dephosphorylation mechanism. It was shown that the chair isomer of ATP^{4-} can be readily converted into the chairPT isomer of ATP^{4-}, but that this process is not likely to occur in the body.

The TG conformer of the β-D-glucose anion was found to be lower in energy than either the GG or GT conformers of the β-D-glucose anion. Without the presence of water molecules, it was determined that the β-D-glucose anion was lowest in energy using the HF/6-31G(d) while the β-L-glucose anion was lowest in energy using other levels of theory. Upon the inclusion of water molecules, it was determined that the β-L-glucose anion was lowest in energy using the B3LYP functional, the α-D-glucose anion was lowest in energy using the HF/6-31G(d) level of theory and the β-D-glucose anion was lowest in energy using the HF/6-31+G(d) level of theory. The ΔU_{rxn}, ΔH_{rxn} and ΔG_{rxn} for

the phosphorylation of deprotonated glucose was least positive for the β-D-glucose anion, both in its normal isomer using HF and in its proton transfer isomer using B3LYP, without the inclusion of water molecules. However, upon the inclusion of water molecules, it was found that the α-L-glucose anion had the least positive ΔU_{rxn}, ΔH_{rxn} and ΔG_{rxn} for the phosphorylation mechanism. It was determined that the process of going from the normal isomer to the proton transfer isomer of the glucose anion is quite favorable, but that this process is unlikely to occur in the body.

There is still a great deal of work that needs to be done. The transition states, the activation energies and the IRCs for the phosphorylation mechanism of deprotonated glucose need to be determined. These will help in verifying the validity of the α-L-glucose anion being involved in the phosphorylation mechanism in the body. The process of converting the β-D-glucose anion into the α-L-glucose anion needs to be explored further, as this would help in determining the feasibility of this conversion in the body and whether the α-L-glucose anion is involved in the phosphorylation mechanism. The deprotonated form of glucose was chosen for study; [20, 21] however, it would be interesting to run the calculations with neutral glucose. This would allow a comparison of results between the two forms of glucose and it would also permit a comparison with previously reported results [23, 26]. The structure of glucose will need to be changed to resemble the simplified model of kanamycin studied by Dr. Arpita Yadav's research group [20], which is simply done by changing the CH_2OH group of glucose into a CH_2NH_2 group and changing the 2'-OH group into a hydroxymethyl group. Also, the calculations need to be performed by solvating the systems and comparing the results to those with individual water molecules added. A key difference is that in solution, the products from

the dephosphorylation of ATP^{4-} become ADP^{3-}, HPO_4^{2-} and H^+ instead of ADP^{3-} and PO_3^- in the gas phase. [19]

Both the Dr. Arpita Yadav and the Dr. Ray Poirier research groups believe that there is a single-step mechanism for this process in the presence of enzymes in which ATP is dephosphorylated as glucose is phosphorylated. [20, 21] This mechanism needs to be explored further by determining the transition states and activation energies. Understanding the phosphorylation mechanism between ATP and glucose can serve as a model for the phosphorylation mechanism between ATP and kanamycin. This understanding can help lead to the development of better antibiotics that would not be susceptible to phosphorylation.

Bibliography and References

1. Alekshun, M. N.; Levy, S. B. Molecular Mechanisms of Antibacterial Multidrug Resistance. *Cell*, **2007**, 128, 1037-1050.

2. Barber, M. Staphylococcal Infection due to Penicillin-resistant Strains. *BMJ*, **1947**, 2, 863-865.

3. Tenover, F.C. Mechanisms of Antimicrobial Resistance in Bacteria. *Am. J. Med.*, **2006**, 119, S3-S10.

4. Okuma, K.; Iwakawa, K.; Turnidge, J. D.; Grubb, W. B.; O'Brien, F. G.; Coombs, G. W.; Pearman, J. W.; Tenover, F. C.; Kapi, M.; Tiensasitorn, C.; Hiramatsu, K. Dissemination of New Methicillin-Resistant Staphylococcus aureus Clones in the Community. *J. Clin. Microbiol.*, **2002**, 40, 4289-4294.

5. Kuwahara, R.; Tsuchiya, T. Synthesis of kanamycin A analogs containing 6-amino-3-oxa-2,3,4,6-tetradeoxy-D and -L-*glycero*-hexopyranose. *Carbohydr. Res.*, **1996**, 286, 107-122.

6. Kobayashi, Y.; Ohgami, T.; Ohtsuki, K.; Tsuchiya, T. Synthesis of kanamycin A analogs containing a 6-amino-6-deoxyglycofuranose moiety. *Carbohydr. Res.*, **2000**, 329, 325-340.

7. Fourmy, D.; Recht, M. I.; Blanchard, S. C.; Puglisi, J. D. Structure of the A Site of *Escherichia coli* 16*S* Ribosomal RNA Complexed with an Aminoglycoside Antibiotic. *Science*, **1996**, 1367-1371.

8. Nishimura, Y.; Tsuchiya, T.; Umezawa, S. *Bull. Chem. Soc. Jpn.*, **1971**, 2521-2528.

9. Azad, C. S.; Bhunia, S. S.; Krishna, A.; Shukla, P. K.; Saxena, A. K. Novel Glycoconjugate of 8-Fluoro Norfloxacin Derivatives as Gentamicin-resistant

Staphylococcus aureus Inhibitors: Synthesis and Molecular Modelling Studies. *Chem. Biol. Drug Des.*, **2015**, 86, 440-446.

10. Amani, J.; Barjini, K. A.; Moghaddam, M. M.; Asadi, A. *In Vitro* Synergistic Effect of the CM11 Antimicrobial Peptide in Combination with Common Antibiotics Against Clinical Isolates of Six Species of Multidrug-Resistant Pathogenic Bacteria. *Protein Pept. Lett.*, **2015**, 22, 940-951.
11. Huang, M.; Wei, K.; Li, X.; McClory, J.; Hu, G.; Zou, J-W.; Timson, D. Phosphorylation Mechanism of Phosphomevalonate Kinase: Implications for Rational Engineering of Isoprenoid Biosynthetic Pathway Enzymes. *J. Phys. Chem. B*, **2016**, 120, 10714-10722.
12. Lu, S.; Deng, R.; Jiang, H.; Song, H.; Li, S.; Shen, Q.; Huang, W.; Nussinov, R.; Yu, J.; Zhang, J. The Mechanism of ATP-Dependent Allosteric Protection of Akt Kinase Phosphorylation. *Structure*, **2015**, 23, 1725-1734.
13. Dehury, B.; Behera, S. K.; Mahapatra, N. Structural dynamics of Casein Kinase I (CKI) from malarial parasite Plasmodium falciparum (Isolate 3D7): Insights from theoretical modelling and molecular simulations. *J. Mol. Graph. Model.*, **2017**, 71, 154-166.
14. Burke, R. M.; Pearce, J. K.; Boxford, W. E.; Bruckmann, A.; Dessent, C. E. H. Stabilization of Excess Charge in Isolated Adenosine 5‘-Triphosphate and Adenosine 5‘-Diphosphate Multiply and Singly Charged Anions. *J. Phys. Chem. A*, **2005**, 109, 9775-9785.

15. Wang, P.; Izatt, R. M.; Oscarson, J. L.; Gillespie, S. E. ^{1}H-NMR Study of Protonation and Mg(II) Coordination of AMP, ADP, and ATP at 25, 50, and 70 °C. *J. Phys. Chem.*, **1996**, 100, 9556-9560.

16. Miyazaki, T.; Kameda, Y.; Umebayashi, Y.; Doi, H.; Amo, Y.; Usuki, T. Conformation of ATP and ADP Molecules in Aqueous Solutions Determined by High-Energy X-ray Diffraction. *J. Solution Chem.*, **2014**, 43, 1487-1498.

17. Bojovschi, A.; Liu, M. S.; Sadus, R. J. Conformational Dynamics of ATP/Mg:ATP in Motor Proteins via Data Mining and Molecular Simulation. *J. Chem. Phys.*, **2012**, 137, 075101.

18. Martínez, L.; Laine, E.; Malliavin, T. E.; Nilges, M.; Blondel, A. ATP Conformations and Ion Binding modes in the Active Site of Anthrax Edema Factor: A Computational Analysis. *Proteins: Struct., Funct., Bioinf.*, **2009**, 77, 971-983.

19. Campbell, N. A.; Reece, J. B.; Urry, L. A.; Cain, M. L.; Wasserman, S. A.; Minorsky, P. V.; Jackson, R. B. "An Introduction to Metabolism" in Biology, 8th ed. San Francisco: Pearson Benjamin Cummings, 2008.

20. Sharma, S.; Walsh, A.; Yadav, A.; Poirier, R.A. Phosphorylation of Kanamycin by ATP Catalyzed via Aminoglycoside Phosphotransferase: A Concerted Nucleophilic Substitution Reaction. In preparation (2018).

21. Sharma, S.; Yadav, A.; Alnakli, J.; Alhamed, S.; Beni, R.; Poirier, R.A. Synthesis and Molecular Docking Study of Aminoglycoside Antibiotic-conjugates to Overcome Drug Resistance. In preparation (2018).

22. Banks, J. L.; Beard, H. S.; Cao, Y.; Cho, A. E.; Damm, W.; Felts, A. K.; Halgren, T. A.; Mainz, D. T.; Maple, J. R.; Murphy, R.; Philipp, D. M.; Reparsky, D.T.; Zhang,

L. Y.; Berne, B. J.; Friesner, R. A.; Gallicchio E.; Levy, R. M. *J. Med. Chem.*, **2004**, 47, 1739-1750.

23. Polavarapu, P. L.; Ewig, C. S. *Ab initio* Computed Molecular Structures and Energies of the Conformers of Glucose. *J. Comput. Chem.*, **1992**, 13, 1255-1261.

24. Ha, S.; Gao, J.; Tidor, B.; Brady, J. W.; Karplus, M. Solvent Effect on the Anomeric Equilibrium in D-glucose: A Free Energy Simulations Analysis. *J. Am. Chem. Soc.*, **1991**, 113, 1553-1557.

25. Chu, S. S. C.; Jeffrey, G. A. The Refinement of the Crystal Structures of β-D-glucose and Cellobiose. *Acta Crystallographica Section B*, **1968**, 24, 830-838.

26. Csonka, G. I.; Éliás, K.; Csizmadia, I. G. Relative Stability of $^{1}C_{4}$ and $^{4}C_{1}$ Chair Forms of β-D-glucose: A Density Functional Study. *Chemical Physics Letters*, **1996**, 257 (1-2), 49-60.

27. Nishida, Y.; Ohrui, H.; Meguro, H. ^{1}H-NMR Studies of (6r)- and (6s)-deuterated D-hexoses: Assignment of the Preferred Rotamers about C5-C6 bond of D-glucose and D-galactose Derivatives in Solution. *Tetrahedron Letters*, **1984**, 25 (15) 1575-1578.

28. Brown, G. M.; Levy, H. A. α-D-Glucose: Further Refinement Based on Neutron-diffraction Data. *Acta Crystallogr. B*, **1979**, 35, 656-659.

29. Polik, W. F.; Schmidt, J. R. WebMO. **2003**, WebMO LLC, Holland, MI, USA.

30. Fritsch, M. J.; Trucks, G. W.; Schlegel, H. B.; Scuseria, G. E.; Robb, M. A.; Cheeseman, J. R.; Scalmani, G.; Barone, V.; Mennucci, B.; Petersson, G. A.; Nakatsuji, H.; Caricato, M.; Li, X.; Hratchian, H. P.; Izmaylov, A. F.; Bloino, J.; Zheng, G.; Sonnenberg, J. L.; Hada, M.; Ehara, M.; Toyota, K.; Fukuda, R.; Hasegawa, J.; Ishida, M.; Nakajima, T.; Honda, Y.; Kitao, O.; Nakai, H.; Vreven, T.;

Montgomery Jr., J.A.; Peralta, J. E.; Ogliaro, F.; Bearpark, M.; Heyd, J. J.; Brothers, E.; Kudin, K. N.; Staroverov, V. N.; Keith, T.; Kobayashi, R.; Normand, J.; Raghavachari, K.; Rendell, A.; Burant, J. C.; Iyengar, S. S.; Tomasi, J.; Cossi, M.; Rega, N.; Millam, J. M.; Klene, M.; Knox, J. E.; Cross, J. B.; Bakken, V.; Adamo, C.; Jaramillo, J.; Gomperts, R.; Stratmann, R. E.; Yazyev, O.; Austin, A. J.; Cammi, R.; Pomelli, C.; Ochterski, J. W.; Martin, R. L.; Morokuma, K.; Zakrzewski, V. G.; Voth, G. A.; Salvador, P.; Dannenberg, J. J.; Dapprich, S.; Daniels, A. D.; Farkas, O.; Foresman, J. B.; Ortiz, J. V.; Cioslowski, J.; Fox, D. J. Gaussian 09, **2013**, Revision E.01, Gaussian Inc., Wallingford, CT.

31. Roothaan, C. C. J. New Developments in Molecular Orbital Theory. *Rev. Mod. Phys.*, **1951**, 23, 69

32. Becke, A. D. Density-functional thermochemistry. III. The role of exact exchange. *J. Chem. Phys.*, **1993**, 98, 5648-5652.

33. Jmol: an open-source Java viewer for chemical structures in 3D. http://www.jmol.org/

34. Campbell, N. A.; Reece, J. B.; Urry, L. A.; Cain, M. L.; Wasserman, S. A.; Minorsky, P. V.; Jackson, R. B. “An Introduction to Metabolism.” in *Biology*, 8th ed. San Francisco: Pearson Benjamin Cummings, 2008.

35. Petrucci, R. H.; Harwood, W. S.; Herring, F. G.; Madura, J. D. “Spontaneous Change: Entropy and Free Energy” in *General Chemistry*, 9th ed. Upper Saddle River: Prentice Hall, 2007.

36. Bruice, P. “The Organic Chemistry of Carbohydrates” in *Organic Chemistry*, 6th ed. Santa Barbara: Prentice Hall, 2011.

37. Bruice, P. “Stereochemistry” in *Organic Chemistry*, 6th ed. Santa Barbara: Prentice Hall, 2011.

38. Sowa, W. Synthesis of L-glucurone. Conversion of D-glucose into L-glucose. *Can. J. Chem.*, **1969**, 47, 3931-3934.

39. Shiozaki, M. Conversion of D-Glucose to L-Glucose: Oxidative Decarboxylation of α-Oxy Carboxylic Acids via Their Diacyl Peroxides. *J. Org. Chem.*, **1991**, 56, 528-532.

Appendices

Appendix I Chair ATP^{4-} PES Scan Energies Using the HF/6-31G(d) Level of Theory (in hartrees)

	Dihedral Degree of Freedom			
Dihedral Angle (°)	2-1-30-31	2-3-13-14	3-4-10-11	3-13-14-15
-170	-2652.13708	-2653.00882	-2653.07806	-2653.08719
-160	-2651.07732	-2652.90187	-2653.08746	-2653.08236
-150	-2648.54883	-2652.78014	-2653.09646	-2653.07893
-140	-2643.31469	-2652.66788	-2653.10543	-2653.07663
-130	-2628.09783	-2652.58916	-2653.11465	-2653.07519
-120	-2607.08400	-2652.49865	-2653.12439	-2653.07444
-110	-2631.22298	-2652.23374	-2653.13479	-2653.07429
-100	-2643.28531	-2651.52741	-2653.14564	-2653.07469
-90	-2649.01384	-2649.97855	-2653.15586	-2653.07570
-80	-2651.28754	-2647.08665	-2653.16346	-2653.07737
-70	-2652.22506	-2646.57954	-2653.16630	-2653.07960
-60	-2652.58597	-2645.21764	-2653.16338	-2653.08184
-50	-2652.71512	-2620.14902	-2653.15523	-2653.08284
-40	-2652.75821	-2643.51712	-2653.14360	-2653.08036
-30	-2652.77773	-2643.33387	-2653.13067	-2653.07175
-20	-2652.80056	-2640.96904	-2653.11829	-2653.05808
-10	-2652.83288	-2648.03049	-2653.10753	-2653.04856
0	-2652.87882	-2652.26611	-2653.09874	-2653.05328
10	-2652.94397	-2652.45996	-2653.09174	-2653.06660
20	-2653.01649	-2652.05878	-2653.08613	-2653.07190
30	-2653.08087	-2650.79323	-2653.08146	-2653.07074
40	-2653.12874	-2649.10200	-2653.07737	-2653.07104
50	-2653.15709	-2650.04210	-2653.07361	-2653.07286
60	-2653.16630	-2651.77147	-2653.07004	-2653.08569
70	-2653.15716	-2652.52859	-2653.06647	-2653.11139
80	-2653.12909	-2652.76846	-2653.06255	-2653.13753
90	-2653.08164	-2652.85330	-2653.05773	-2653.15770
100	-2653.01742	-2652.91598	-2653.05143	-2653.16630
110	-2652.94437	-2652.97959	-2653.04344	-2653.15976
120	-2652.87807	-2653.03770	-2653.03452	-2653.14896
130	-2652.83167	-2653.08636	-2653.02727	-2653.13694
140	-2652.79908	-2653.12541	-2653.02575	-2653.12580
150	-2652.77543	-2653.15414	-2653.03210	-2653.11656
160	-2652.75241	-2653.16630	-2653.04364	-2653.10818
170	-2652.70041	-2653.14907	-2653.05622	-2653.10042

180	-2652.54970	-2653.09361	-2653.06778	-2653.09335

	Dihedral Degree of Freedom		
Dihedral Angle (°)	4-5-7-8	16-17-18-19	17-18-19-20
-170	-2653.13359	-2653.16630	-2652.97394
-160	-2653.13396	-2653.16593	-2653.06828
-150	-2653.13411	-2653.16486	-2653.12539
-140	-2653.13418	-2653.16325	-2653.15642
-130	-2653.13436	-2653.16130	-2653.16630
-120	-2653.13484	-2653.15923	-2653.15648
-110	-2653.13573	-2653.15725	-2653.12597
-100	-2653.13709	-2653.15550	-2653.07053
-90	-2653.13886	-2653.15402	-2652.98018
-80	-2653.14098	-2653.15272	-2652.83907
-70	-2653.14333	-2653.15140	-2652.76852
-60	-2653.14584	-2653.14983	-2652.73925
-50	-2653.14847	-2653.14781	-2652.47843
-40	-2653.15122	-2653.14523	-2651.30857
-30	-2653.15414	-2653.14206	-2646.26355
-20	-2653.15725	-2653.13848	-2617.44453
-10	-2653.16043	-2653.13507	-2308.10103
0	-2653.16336	-2653.13261	-2613.47970
10	-2653.16550	-2653.13180	-2645.60613
20	-2653.16630	-2653.13286	-2651.17812
30	-2653.16543	-2653.13545	-2652.39405
40	-2653.16288	-2653.13886	-2652.61147
50	-2653.15892	-2653.14234	-2652.55659
60	-2653.15404	-2653.14545	-2652.60889
70	-2653.14875	-2653.14803	-2652.46293
80	-2653.14353	-2653.15010	-2651.47378
90	-2653.13875	-2653.15171	-2646.98003
100	-2653.13472	-2653.15299	-2621.07800
110	-2653.13166	-2653.15419	-1933.17550
120	-2653.12971	-2653.15554	-2603.72064
130	-2653.12886	-2653.15719	-2644.47874
140	-2653.12896	-2653.15914	-2650.95829
150	-2653.12973	-2653.16122	-2652.39836
160	-2653.13083	-2653.16320	-2652.72321
170	-2653.13196	-2653.16484	-2652.76696
180	-2653.13292	-2653.16592	-2652.82992

Appendix II Linear ATP^{4-} PES Scan Energies using the HF/6-31G(d) level of theory (in hartrees)

	Dihedral Degree of Freedom			
Dihedral Angle (°)	1-5-6-7	1-28-29-30	2-1-28-29	4-3-12-13
-170	-2653.10043	-2653.08367	-2652.86519	-2652.33182
-160	-2653.10476	-2653.08297	-2652.71203	-2652.62668
-150	-2653.11405	-2653.08357	-2652.61090	-2652.73506
-140	-2653.12045	-2653.08515	-2652.62057	-2652.77658
-130	-2653.12681	-2653.08728	-2652.59094	-2652.80137
-120	-2653.13319	-2653.08943	-2652.32500	-2652.82722
-110	-2653.13954	-2653.08896	-2651.44018	-2652.86266
-100	-2653.14561	-2653.07802	-2649.77878	-2652.92510
-90	-2653.15088	-2653.04706	-2649.58983	-2653.00223
-80	-2653.15457	-2652.99189	-2651.27042	-2653.06949
-70	-2653.15593	-2652.89070	-2652.27818	-2653.11800
-60	-2653.15450	-2652.53639	-2652.59670	-2653.14648
-50	-2653.15028	-2651.82315	-2652.63991	-2653.15593
-40	-2653.14374	-2647.21405	-2652.61118	-2653.14604
-30	-2653.13583	-2649.12529	-2652.60096	-2653.11552
-20	-2653.12765	-2649.70544	-2652.60096	-2653.06525
-10	-2653.12016	-2638.29900	-2652.61635	-2653.00008
0	-2653.11385	-2627.55577	-2652.57473	-2652.92924
10	-2653.10878	-2646.09686	-2652.27148	-2652.86590
20	-2653.10472	-2651.82689	-2651.29133	-2652.81735
30	-2653.10132	-2652.63817	-2649.68472	-2652.77968
40	-2653.09823	-2652.96576	-2649.98504	-2652.75035
50	-2653.09515	-2653.09981	-2651.62793	-2652.73898
60	-2653.09179	-2653.14669	-2652.47912	-2652.72831
70	-2653.08782	-2653.15593	-2652.76445	-2652.67843
80	-2653.08289	-2653.15096	-2652.92812	-2652.51212
90	-2653.07670	-2653.14029	-2652.99170	-2652.05462
100	-2653.06914	-2653.12868	-2653.04770	-2650.91111
110	-2653.06079	-2653.11836	-2653.09221	-2648.33212
120	-2653.05349	-2653.10974	-2653.12549	-2643.09362
130	-2653.05038	-2653.10294	-2653.14763	-2630.14606
140	-2653.05389	-2653.09778	-2653.15593	-2621.03426
150	-2653.06278	-2653.09385	-2653.14675	-2636.99746
160	-2653.07350	-2653.09070	-2653.11871	-2645.76975
170	-2653.08368	-2653.08795	-2653.06869	-2649.68779
180	-2653.09262	-2653.08551	-2652.98669	-2651.56569

	Dihedral Degree of Freedom		
Dihedral Angle (°)	5-4-10-11	31-32-35-36	32-35-36-37
-170	-2653.13039	-2653.15593	-2652.38740
-160	-2653.13101	-2653.15558	-2650.94891
-150	-2653.13142	-2653.15458	-2644.48555
-140	-2653.13175	-2653.15306	-2604.19920
-130	-2653.13218	-2653.15119	-2097.12187
-120	-2653.13286	-2653.14918	-2621.46148
-110	-2653.13390	-2653.14725	-2647.01134
-100	-2653.13531	-2653.14552	-2651.46705
-90	-2653.13705	-2653.14405	-2652.44428
-80	-2653.13900	-2653.14273	-2652.58498
-70	-2653.14107	-2653.14136	-2652.54131
-60	-2653.14317	-2653.13972	-2652.58874
-50	-2653.14528	-2653.13766	-2652.33128
-40	-2653.14743	-2653.13511	-2650.96516
-30	-2653.14964	-2653.13215	-2644.54691
-20	-2653.15186	-2653.12910	-2605.29368
-10	-2653.15389	-2653.12656	-2015.80831
0	-2653.15537	-2653.12517	-2619.86848
10	-2653.15593	-2653.12530	-2646.73866
20	-2653.15532	-2653.12687	-2651.40607
30	-2653.15348	-2653.12939	-2652.49377
40	-2653.15055	-2653.13225	-2652.73548
50	-2653.14681	-2653.13499	-2652.76171
60	-2653.14258	-2653.13740	-2652.83763
70	-2653.13824	-2653.13943	-2652.97328
80	-2653.13408	-2653.14110	-2653.06175
90	-2653.13037	-2653.14245	-2653.11620
100	-2653.12736	-2653.14361	-2653.14624
110	-2653.12523	-2653.14476	-2653.15593
120	-2653.12408	-2653.14608	-2653.14615
130	-2653.12390	-2653.14765	-2653.11539
140	-2653.12449	-2653.14945	-2653.05864
150	-2653.12561	-2653.15133	-2652.96470
160	-2653.12696	-2653.15312	-2652.82266
170	-2653.12831	-2653.15460	-2652.75979
180	-2653.12949	-2653.15559	-2652.71418

Appendix III ATP^{4-} Dephosphorylation Data Using the HF/6-31G(d) Level of Theory

Isomer	**Energy (hartrees)**	**Enthalpy (hartrees)**	**Entropy ($J\ mol^{-1}\ K^{-1}$)**	**Gibbs Energy ($kJ\ mol^{-1}$)**
Chair ATP^{4-}	-2653.1711357	-2652.838327	783.864	-6.965261E06
Linear ATP^{4-}	-2653.1559328	-2652.821253	824.206	-6.965228E06
ChairPT ATP^{4-}	-2653.2473191	-2652.914687	796.349	-6.965465E06
Chair $ATP^{4-}\cdot 4H_2O$	-2957.4234733	-2956.968256	984.190	-7.763590E06
Linear $ATP^{4-}\cdot 4H_2O$	-2957.4111895	-2956.955114	980.106	-7.763555E06
ChairPT $ATP^{4-}\cdot 4H_2O$	-2957.4625166	-2957.009449	1040.272	-7.763702E06
Chair $ATP^{4-}\cdot 5H_2O$	-3033.4757052	-3032.990481	1047.268	-7.963429E06
ChairPT ATP^{4-} TS	-2653.2462926	-2652.914691	791.286	-6.965463E06
Chair $ATP^{4-}\cdot 4H_2O$ TS	-2957.3782474	-2956.926840	1042.121	-7.763486E06
ChairPT $ATP^{4-}\cdot 4H_2O$ TS	-2957.3925356	-2956.941060	1057.314	-7.764709E06
Chair $ATP^{4-}\cdot 5H_2O$ TS	-3033.4317264	-3032.949731	1102.969	-7.963338E06
ChairPT ATP^{4-} Products	-2653.4595524	-2653.126588	956.027	-6.966069E06
Chair $ATP^{4-}\cdot 4H_2O$ Products	-2957.5743438	-2957.122880	1212.636	-7.764013E06
ChairPT $ATP^{4-}\cdot 4H_2O$ Products	-2957.6378336	-2957.186912	1231.544	-7.764182E06
Chair $ATP^{4-}\cdot 5H_2O$ Products	-3033.6252218	-3033.143038	1268.208	-7.963895E06

Appendix IV ATP^{4-} Dephosphorylation Data Using the HF/6-31+G(d) Level of Theory

Isomer	**Energy (hartrees)**	**Enthalpy (hartrees)**	**Entropy (J mol^{-1} K^{-1})**	**Gibbs Energy (kJ mol^{-1})**
Chair ATP^{4-}	-2653.2842819	-2652.952111	787.215	-6.965560E06
Linear ATP^{4-}	-2653.2721032	-2652.938786	791.136	-6.965527E06
ChairPT ATP^{4-}	-2653.3569541	-2653.025269	798.094	-6.965756E06
Chair $ATP^{4-}\cdot 4H_2O$	-2957.5491165	-2957.095100	989.311	-7.764148E06
Linear $ATP^{4-}\cdot 4H_2O$	-2957.5382920	-2957.083380	982.052	-7.764115E06
ChairPT $ATP^{4-}\cdot 4H_2O$	-2957.5899970	-2957.138109	1045.941	-7.764278E06
ChairPT ATP^{4-} TS	-2653.3544022	-2653.023770	796.726	-6.965751E06
Chair $ATP^{4-}\cdot 4H_2O$ TS	-2957.5032797	-2957.052889	1051.732	-7.764056E06
ChairPT $ATP^{4-}\cdot 4H_2O$ TS	-2957.5170636	-2957.067142	1073.589	-7.764100E06
ChairPT ATP^{4-} Products	-2653.5671586	-2653.236828	962.692	-6.966360E06
Chair $ATP^{4-}\cdot 4H_2O$ Products	-2957.7015973	-2957.251209	1216.946	-7.764626E06
ChairPT $ATP^{4-}\cdot 4H_2O$ Products	-2957.7637806	-2957.314138	1240.836	-7.764798E06

Appendix V ATP^{4-} Dephosphorylation Data Using the B3LYP/6-31G(d) Level of Theory

Isomer	**Energy (hartrees)**	**Enthalpy (hartrees)**	**Entropy (J mol^{-1} K^{-1})**	**Gibbs Energy (kJ mol^{-1})**
Chair $ATP^{4-}\cdot 4H_2O$	-2969.7873973	-2969.367801	1016.402	-7.796378E06
Linear $ATP^{4-}\cdot 4H_2O$	-2969.7750231	-2969.354355	1015.511	-7.796343E06
ChairPT $ATP^{4-}\cdot 4H_2O$	-2969.8222754	-2969.402591	1069.857	-7.796485E06
ChairPT $ATP^{4-}\cdot 4H_2O$ TS	-2969.7610553	-2969.343176	1080.162	-7.796333E06
ChairPT $ATP^{4-}\cdot 4H_2O$ Products	-2970.0005897	-2969.582752	1251.731	-7.797013E06

Appendix VI ATP^{4-} Dephosphorylation Data Using the B3LYP/6-31+G(d) Level of Theory

Isomer	**Energy (hartrees)**	**Enthalpy (hartrees)**	**Entropy (J mol^{-1} K^{-1})**	**Gibbs Energy (kJ mol^{-1})**
Chair $ATP^{4-}\cdot 4H_2O$	-2969.9938035	-2969.574984	1021.181	-7.796924E06
Linear $ATP^{4-}\cdot 4H_2O$	-2969.9839530	-2969.563804	1009.704	-7.796891E06
ChairPT $ATP^{4-}\cdot 4H_2O$	-2970.0327600	-2969.614605	1077.857	-7.797045E06
ChairPT $ATP^{4-}\cdot 4H_2O$ TS				
ChairPT $ATP^{4-}\cdot 4H_2O$ Products	-2970.2108439	-2969.794554	1263.468	-7.797572E06

Appendix VII Glucose Anion Phosphorylation Data Using the HF/6-31G(d) Level of Theory

Anion Form	**Energy (hartrees)**	**Enthalpy (hartrees)**	**Entropy (J mol^{-1} K^{-1})**	**Gibbs Energy (kJ mol^{-1})**
α-D-glucose Reactants	-1248.1412816	-1247.912946	689.916	-3.276601E06
α-L-glucose Reactants	-1248.1403316	-1247.912011	689.732	-3.276599E06
β-D-glucose Reactants	-1248.1411807	-1247.913273	694.477	-3.276603E06
β-L-glucose Reactants	-1248.1413370	-1247.913487	694.632	-3.276604E06
α-D-glucose·H_2O Reactants	-1400.2189125	-1399.930297	838.260	-3.675767E06
α-L-glucose·H_2O Reactants	-1400.2181511	-1399.929295	826.834	-3.675761E06
β-D-glucose·H_2O Reactants	-1400.2185452	-1399.930352	843.486	-3.675769E06
β-L-glucose·H_2O Reactants	-1400.2185371	-1399.930078	828.888	-3.675764E06
Phosphorylated α-D-glucose	-1248.0959288	-1247.864839	500.210	-3.276418E06
Phosphorylated α-L-glucose	-1248.0953875	-1247.863642	500.097	-3.276415E06
Phosphorylated β-D-glucose	-1248.0979132	-1247.867280	503.850	-3.276426E06
Phosphorylated β-L-glucose	-1248.0963763	-1247.865057	499.996	-3.276419E06
Phosphorylated α-D-glucose·$2H_2O$	-1400.1982005	-1399.905570	620.596	-3.675637E06
Phosphorylated α-L-glucose·$2H_2O$	-1400.2042684	-1399.910360	589.191	-3.675640E06
Phosphorylated β-D-glucose·$2H_2O$	-1400.2000656	-1399.907729	624.558	-3.675644E06
Phosphorylated β-L-glucose·$2H_2O$	-1400.1987076	-1399.905956	616.722	-3.675637E06

Appendix VIII Glucose Anion Phosphorylation Data Using the HF/6-31+G(d) Level of Theory

Anion Form	Energy (hartrees)	Enthalpy (hartrees)	Entropy (J mol^{-1} K^{-1})	Gibbs Energy (kJ mol^{-1})
α-D-glucose Reactants	-1248.2024169	-1247.974345	691.762	-3.276763E06
α-L-glucose Reactants	-1248.2017292	-1247.973707	691.632	-3.276761E06
β-D-glucose Reactants	-1248.2036796	-1247.976054	696.565	-3.276769E06
β-L-glucose Reactants	-1248.2036188	-1247.976031	697.423	-3.276769E06
α-D-glucose·H_2O Reactants	-1400.2896266	-1400.001623	845.858	-3.675956E06
α-L-glucose·H_2O Reactants	-1400.2891064	-1400.001117	841.825	-3.675954E06
β-D-glucose·H_2O Reactants	-1400.2906720	-1400.003109	849.925	-3.675962E06
β-L-glucose·H_2O Reactants	-1400.2906001	-1400.003035	847.369	-3.675961E06
Phosphorylated α-D-glucose	-1248.1537731	-1247.922823	503.670	-3.276572E06
Phosphorylated α-L-glucose	-1248.1526830	-1247.921391	501.842	-3.276567E06
Phosphorylated β-D-glucose	-1248.1568169	-1247.926291	508.465	-3.276582E06
Phosphorylated β-L-glucose	-1248.1550264	-1247.923975	502.281	-3.276574E06
Phosphorylated α-D-glucose·$2H_2O$	-1400.2643048	-1399.972579	627.215	-3.675815E06
Phosphorylated α-L-glucose·$2H_2O$	-1400.2668167	-1399.973723	594.894	-3.675808E06
Phosphorylated β-D-glucose·$2H_2O$	-1400.2671509	-1399.975788	631.307	-3.675825E06
Phosphorylated β-L-glucose·$2H_2O$	-1400.2647474	-1399.969202	627.424	-3.675806E06

Appendix IX Glucose Anion Phosphorylation Data Using the B3LYP/6-31G(d) Level of Theory

Anion Form	**Energy (hartrees)**	**Enthalpy (hartrees)**	**Entropy (J mol^{-1} K^{-1})**	**Gibbs Energy (kJ mol^{-1})**
α-D-glucose PT Reactants	-1253.7098924	-1253.497900	703.184	-3.291268E06
α-L-glucose PT Reactants	-1253.7086537	-1253.496591	701.803	-3.291265E06
β-D-glucose PT Reactants	-1253.7095851	-1253.497794	705.468	-3.291269E06
β-L-glucose PT Reactants	-1253.7110657	-1253.499200	705.280	-3.291272E06
α-D-glucose·H_2O Reactants	-1406.5813058	-1406.314681	846.151	-3.692531E06
α-L-glucose·H_2O Reactants	-1406.5824485	-1406.315718	824.662	-3.692528E06
β-D-glucose·H_2O Reactants	-1406.5798183	-1406.313539	847.791	-3.692529E06
β-L-glucose·H_2O PT Reactants	-1406.5930054	-1406.324249	823.235	-3.692550E06
Phosphorylated α-D-glucose PT	-1253.6599692	-1253.446248	516.573	-3.291077E06
Phosphorylated α-L-glucose PT	-1253.6573160	-1253.443809	519.967	-3.291072E06
Phosphorylated β-D-glucose PT	-1253.6602894	-1253.447084	527.812	-3.291083E06
Phosphorylated β-L-glucose PT	-1253.6574375	-1253.444187	523.799	-3.291074E06
Phosphorylated α-D-glucose·$2H_2O$	-1406.5543054	-1406.284215	624.859	-3.692386E06
Phosphorylated α-L-glucose·$2H_2O$	-1406.5679395	-1406.296141	591.003	-3.692407E06
Phosphorylated β-D-glucose·$2H_2O$	-1406.5560714	-1406.285826	625.152	-3.692390E06
Phosphorylated β-L-glucose·$2H_2O$	-1406.5549632	-1406.284250	620.094	-3.692384E06

Appendix X Glucose Anion Phosphorylation Data Using the B3LYP/6-31+G(d) Level of Theory

Anion Form	**Energy (hartree)**	**Enthalpy (hartree)**	**Entropy (J mol^{-1} K^{-1})**	**Gibbs Energy (kJ mol^{-1})**
α-D-glucose PT Reactants	-1253.8106645	-1253.599213	706.008	-3.291535E06
α-L-glucose PT Reactants	-1253.8099200	-1253.598516	706.268	-3.291533E06
β-D-glucose PT Reactants	-1253.8118415	-1253.600676	709.125	-3.291540E06
β-L-glucose PT Reactants	-1253.8128724	-1253.601627	709.163	-3.291543E06
α-D-glucose·H_2O Reactants	-1406.7024281	-1406.436550	851.959	-3.692853E06
α-L-glucose·H_2O Reactants	-1406.7012882	-1406.435585	853.666	-3.692851E06
β-D-glucose·H_2O Reactants	-1406.7025455	-1406.437122	854.143	-3.692855E06
β-L-glucose·H_2O Reactants	-1406.7027995	-1406.437401	858.410	-3.692857E06
Phosphorylated α-D-glucose PT	-1253.7525073	-1253.539826	534.117	-3.291328E06
Phosphorylated α-L-glucose PT	-1253.7509193	-1253.538024	525.402	-3.291321E06
Phosphorylated β-D-glucose PT	-1253.7565977	-1253.543780	526.736	-3.291336E06
Phosphorylated β-L-glucose PT	-1253.7527097	-1253.540069	527.611	-3.291327E06
Phosphorylated α-D-glucose·$2H_2O$	-1406.6666432	-1406.397899	645.240	-3.692690E06
Phosphorylated α-L-glucose·$2H_2O$	-1406.6734882	-1406.402923	602.145	-3.692690E06
Phosphorylated β-D-glucose·$2H_2O$	-1406.6691398	-1406.400664	645.524	-3.692697E06
Phosphorylated β-L-glucose·$2H_2O$	-1406.6666158	-1406.397355	633.704	-3.692685E06